Visually Descriptive Language Model for Vector Graphics Reasoning

Zhenhailong Wang[1], Joy Hsu[2], Xingyao Wang[1], Kuan-Hao Huang[1,3], Manling Li[2,4], Jiajun Wu[2], Heng Ji[1]
[1]University of Illinois Urbana-Champaign, [2]Stanford University, [3]Texas A&M University, [4]Northwestern University
{wangz3, xingyao6, khhuang, hengji}@illinois.edu
{joycj, manlingl}@stanford.edu, jiajunwu@cs.stanford.edu

Reviewed on OpenReview: `https://openreview.net/forum?id=WzS33L1iPC`

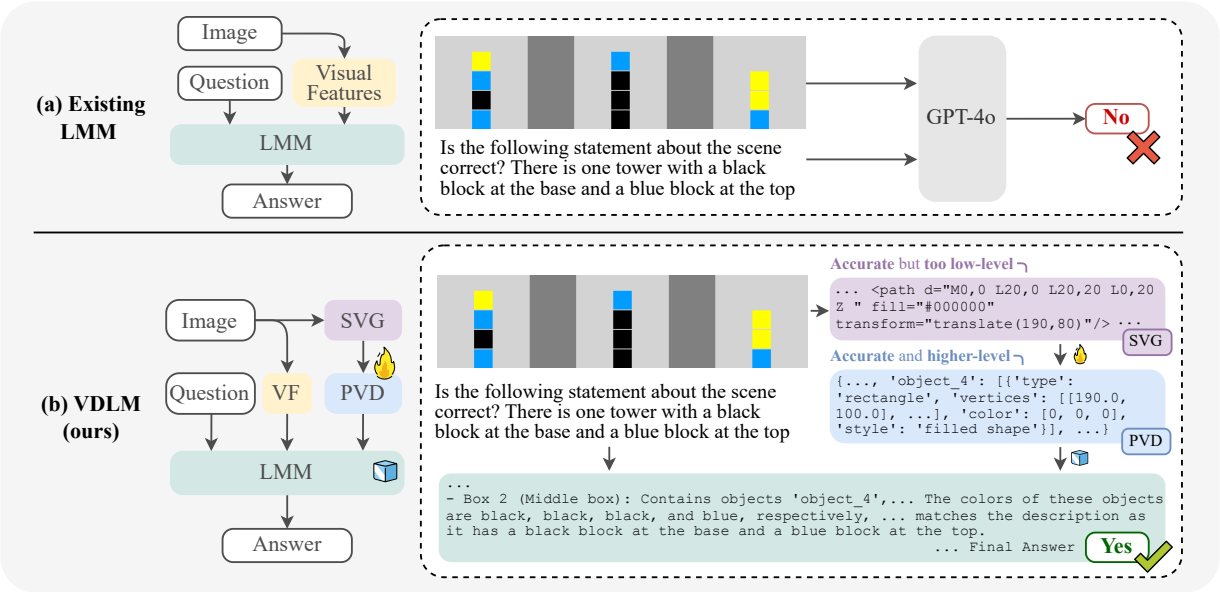

Figure 1: Existing monolithic LMMs rely solely on pretrained vision encoders, such as CLIP (Radford et al., 2021), for perception, which often fail to accurately capture low-level visual details in vector graphics-style images. In contrast, VDLM enables precise visual reasoning by introducing SVG encoding and a learned intermediate symbolic representation, Primal Visual Description (PVD), that bridges low-level SVG perception with high-level language reasoning. "VF" in (b) refers to "visual features".

Abstract

Despite significant advancements, current large multimodal models (LMMs) struggle to bridge the gap between low-level visual perception—focusing on shapes, sizes, and layouts—and high-level language reasoning involving semantics, events, and logic. This limitation becomes evident in tasks requiring precise visual perception, such as comparing geometric properties or solving visual algorithmic reasoning problems. To study this failure mode, we focus on an important visual domain: vector graphics—images composed purely of 2D objects and shapes, which are prevalent in web and mobile environments. Importantly, we consider *rasterized* vector graphics without assuming access to their underlying vector code. We identify two key research questions: how can we enable precise visual perception, and how can we facilitate high-level reasoning based on such low-level perceptions? To accurately capture low-level visual details, we explore using SVG for the precise encoding of

visual scenes. However, SVGs are not readily interpretable by LLMs or LMMs in a zero-shot manner. To address this challenge, we propose the **Visually Descriptive Language Model (VDLM)** to build a bridge between low-level visual perception and high-level language reasoning. VDLM learns an intermediate symbolic representation called **Primal Visual Description (PVD)**, which translates raw SVGs into a higher-level abstraction comprising primitive attributes. This abstraction allows for *direct interpretation* by foundation models for zero-shot generalization to different reasoning tasks. As an initial step to construct a descriptive intermediate representation for low-level visual reasoning, the SVG-to-PVD model is currently limited to simple compositions of primitive shapes, for which synthetic data can be generated without human annotation. Nevertheless, empirical experiments show that VDLM leads to significant improvements in state-of-the-art LMMs, such as GPT-4o, across various low-level multimodal perception and reasoning tasks on rasterized vector graphics. Additionally, we provide extensive analyses of VDLM's performance, showing that our framework offers improved interpretability due to its disentangled perception and reasoning processes. We also conduct an in-depth error analysis, highlighting remaining limitations and suggesting directions for future research.

1 Introduction

In recent years, large multimodal models (LMMs) (OpenAI, 2023b; Anil et al., 2023; Liu et al., 2023b; Chen et al., 2023b; Bai et al., 2023) have achieved impressive performance across a wide spectrum of general vision-language benchmarks (Goyal et al., 2017; Fu et al., 2023; Liu et al., 2023d; Yu et al., 2023; Li et al., 2023a). However, these monolithic LMMs still struggle with seemingly simple tasks that require precise perception of low-level visual details. In particular, we empirically observe that LMMs frequently exhibit this failure mode in vector graphics, which are images composed purely of 2D objects and shapes. For example, a state-of-the-art LMM like GPT-4o (OpenAI, 2024) can still fail 43% of the time when comparing the lengths of two line segments, and 54% of the time when solving a simple 2×2 maze. LMMs' ability to understand vector graphics is largely underexplored compared to natural images but is essential for growing downstream applications in web, visual design, and OS environments (Zhou et al., 2023b; Liu et al., 2024; Xie et al., 2024; Rawles et al., 2024; Zheng et al., 2024; Lù et al., 2024). In this work, we focus on the fundamental aspects of low-level visual reasoning involving vector graphics—including measurements, spatial relations, counting, and logical reasoning. It is important to note that in this paper, "vector graphics" refers to **rasterized images** in JPEG or PNG format, without assuming access to their underlying vector code. This reflects a more realistic setting for visual reasoning in real-world scenarios, such as web Zhou et al. (2023b); Lù et al. (2024) and mobile Wang et al. (2024; 2025). To address the aforementioned challenge, we identify two main research questions. First, how can we enable precise visual perception in LMMs? Second, how can we bridge the gap between low-level perception and high-level reasoning?

For our initial question, we explore encoding a rasterized image via vectorization with SVG representation, which describes a scene with paths (e.g., polygons and splines) and their corresponding measurements and positions. SVG representations, by nature, are unbiased towards high-level semantics and can capture low-level visual details in text. The vectorization process can be faithfully accomplished with an rule-based raster-to-vector algorithm. However, such machine-generated SVG is often noisy and far from natural language, making it insufficient for language reasoning. Our preliminary experiments (§A) demonstrate that existing foundation models are unable to interpret machine-generated SVG codes in zero-shot settings. Another key challenge lies in the scarcity of end-to-end instruction tuning data containing ⟨SVG, question, answer⟩ triplets, making direct fine-tuning infeasible.

To bridge this perception-reasoning gap and address data scarcity, we propose translating the low-level SVG paths to a higher-level intermediate symbolic representation, referred to as **Primal Visual Description (PVD)**, which can directly be leveraged by foundation models for multimodal reasoning. Specifically, we learn an LLM-based (Jiang et al., 2023) SVG-to-PVD model, which transforms the raw SVG paths into a set of primitive attributes (e.g., shape, position) with corresponding predicted values (e.g., rectangle, pixel coordinates of the vertices). See Figure 1 in the blue box for an example. Notably, the PVD representation

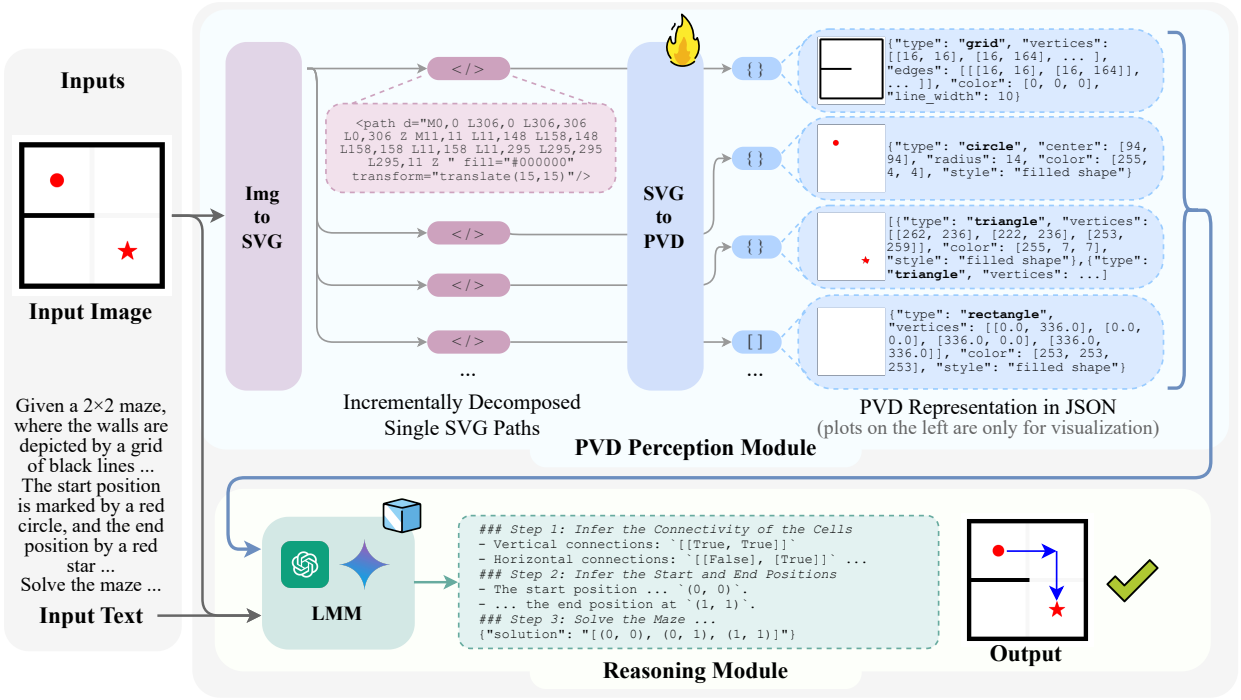

Figure 2: An example of VDLM during inference. First, VDLM extracts individual SVG paths from the input image and then transforms them into Primal Visual Description (PVD) using a trained language model. These PVD perception results, along with the input text queries and the original input image, are subsequently fed into an LMM for reasoning. It is worth noting that although a "star" (★) is not explicitly part of the PVD primitive ontology (see Figure 3), the SVG-to-PVD model can approximate the "star" by composing two triangles (★). A strong off-the-shelf reasoner, such as GPT-4 (OpenAI, 2023a), can accurately deduce that this composition corresponds to the "star," which is the target end position of the maze. For the complete response, refer to Figure 17.

consists of primitive attributes that serve as fundamental building blocks for vector graphics, enabling learning from procedurally synthesized ⟨SVG, PVD⟩ pairs without requiring task-specific annotations. PVD filters out unnecessary noise in SVGs, enhancing the semantics of perception and facilitating subsequent reasoning. Currently, we limit the scope of the SVG-to-PVD model to simple compositions of geometric primitives, for which synthetic data can be generated without human annotation. We leave generalization to entirely open-domain images as future work.

Comprising SVG-based image perception and PVD abstractions, we present the **Visually Descriptive Language Model (VDLM)**, which contains three components: a rule-based visual encoder that converts images to SVG to capture precise visual details, a learned language model that translates SVG to PVD, and an inference-only reasoner that conducts zero-shot reasoning about downstream tasks with the PVD representation. An overview of VDLM is provided in Figure 1. Experimental results demonstrate that VDLM achieves strong zero-shot performance in various visual reasoning tasks, outperforming LLaVA-v1.5 (Liu et al., 2023a), G-LLaVA (Gao et al., 2023), GPT-4V (OpenAI, 2023b), GPT-4o (OpenAI, 2024), and Visual Programming approaches such as ViperGPT (Surís et al., 2023). Moreover, VDLM also enhances interpretability through better disentanglement of perception and reasoning processes.

To summarize, the key contributions of our work are threefold: First, we identify a critical failure mode of LMMs when reasoning about tasks that require precise, low-level perception. Second, we introduce VDLM, the first attempt to enhance LMMs' fine-grained visual reasoning capabilities with vectorized and symbolic visual descriptions—SVG representations and learned Primal Visual Description. Finally, we present an in-depth analysis of the emergent patterns, the disentangled impact of PVD quality on end-task performance, and the remaining limitations, highlighting directions for future work.

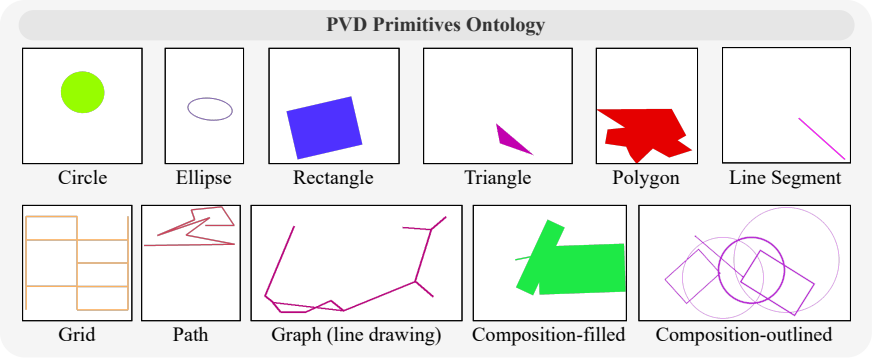

Figure 3: Ontology of the primitives in PVD. Composition of fundamental building blocks for vector graphics, as shown in Figure 4.

2 VDLM Framework

We introduce the VDLM framework, which consists of three main components. First, a rule-based perception module converts images into SVG format, capturing low-level visual details (§ 2.1) that are highly complementary to CLIP-like image features. Second, a trained language model aligns SVGs with intermediate visual descriptions (§ 2.2). Third, an inference-only foundational model reasons about downstream tasks using both visual and textual perception results (§ 2.3). Refer to Figure 2 for an overview of VDLM.

2.1 Precise Visual Perception with SVG Encoding

Prior work (Krojer et al., 2022; Tong et al., 2024) has demonstrated that, although CLIP-based (Radford et al., 2021) vision encoders are effective at capturing high-level visual semantics, they can fall short in preserving fine-grained visual details. We propose extracting an SVG representation that more accurately captures detailed measurements and is highly complementary to the widely used visual features. This can be achieved using rule-based image-to-SVG converters, such as Vtracer VTracer (2024), for which we empirically observe near-perfect reconstruction quality on rasterized vector graphic images (see detailed analysis in Appendix D). SVG describes shapes, lines, and colors using mathematical expressions and paths with precise coordinates.

We conduct a suite of preliminary experiments (§ A) to investigate the potential of using SVG for representing visual inputs. We empirically observe that SVG representation outperforms CLIP-based features on low-level vector graphics reasoning tasks given sufficient task-specific fine-tuning data. However, two key challenges remain (§ A.3): First, off-the-shelf foundation models, such as GPT-4 (OpenAI, 2023a), have limited zero-shot reasoning abilities when dealing with raw SVG code. Second, obtaining task-specific ⟨SVG, question, answer⟩ data for fine-tuning is extremely challenging, which restricts generalization to unseen tasks and domains. We discuss how we address these challenges by learning an intermediate abstraction.

2.2 Bridging Low-Level Visual Perception with High-Level Language Reasoning

Primal Visual Description (PVD). We propose Primal Visual Description, a higher-level abstraction that transforms low-level SVG paths to more structured primitives required for reasoning. PVD is a text-based visual description that consists of a set of primitive geometry objects, e.g., circles and line segments. Each PVD element contains the primitives' attributes (e.g., color, shape, position, size) with corresponding predicted values (e.g., blue, circle, pixel coordinates of the center, length of the radius). An example of the PVD representation is as follows (See Figure 14 for full definitions):

```
{"type": "circle", "center": [252, 315],
 "radius": 202, "color": [175, 155, 98],
 "style": "filled shape"}.
```

Unlike raw SVG code, PVD can be *directly reasoned about* by strong off-the-shelf foundation models to generalize across various downstream tasks. Moreover, PVD is sufficient to serve as a unified visual description across different types of vector graphics, as complex concepts can be composed of multiple primitive shapes. For example, a "cross" can be composed of two "rectangles." As shown in Figure 3, the ontology of the Primal Visual Description contains 9 canonical primitive shape types that can be composed to cover various vector graphics in the wild. The primitive shapes include circles, ellipses, rectangles, triangles, polygons, line segments, grids, paths, and graphs. A path in PVD is defined as a non-intersecting polyline. Graphs and grids are defined as a set of vertices connected by a set of edges. As an initial step to build a visually descriptive intermediate representation, we focus on demonstrating proof of concept; extension to a more comprehensive ontology will be left for future work.

Learning SVG-to-PVD alignment with a language model. We then train a language model to generate PVD outputs from SVG inputs. The input is a single SVG path depicting a visual concept, and the output is the predicted one or more primitives in the defined PVD ontology. During inference, given an arbitrary raster image, we first convert it into a raw SVG file, which may contain a large number of SVG paths, including noise and speckles. To denoise the raw SVG file and extract salient shapes, we propose an incremental decomposition algorithm. Specifically, we incrementally include SVG paths while checking the difference between the partially rendered image of currently chosen paths and the fully rendered image of the original raw SVG file. We compute the summation of the absolute pixel-by-pixel difference between the two images and set an empirical threshold. If the difference after adding a new path is below this threshold, i.e., if the added path does not bring much additional visual information to the scene, we will skip that path. For the ordering of the path selection, we follow the default ordering from VTracer (2024) that heuristically places the paths with a larger area at the front. The paths that come afterward will be stacked on top of previous paths during rendering. Upon obtaining the decomposed single SVG paths, we first generate their PVD representation individually. We then aggregate the individual PVD predictions into a holistic perception of the entire image using this JSON template: `["object_0": <PVD output for path 0>, "object_1": <PVD output for path 1>, ...]`.

Importantly, since PVD is **task-agnostic**, the data for training the SVG-to-PVD model can be procedurally generated without human annotation. We develop a data generator leveraging PIL.ImageDraw and VTracer (2024), which creates a large-scale ⟨SVG, PVD⟩ paired dataset containing randomly generated primitives. In some real-world tasks, such as geometry problems, multiple primitive shapes with the same color can overlap. When converted to SVG, these shapes tend to be parsed into one merged SVG path. To enable the SVG-to-PVD model to learn to decode individual primitives from such compositional concepts, we additionally generate data instances with randomly overlapped shapes. The target PVD representation, in this context, is a list of primitive PVD JSON objects. We ensure that each generated image contains only one unicolor object, single or composed, so that the converted SVG contains a single SVG path. This facilitates a language model in effectively learning the alignment between SVG and PVD.

To improve the robustness to unseen inference images, we randomize the image sizes, the positions and rotations of the shapes, as well as the styles of the shapes (filled or outlined). We additionally use two data augmentation methods, Gaussian Blur and Pixel Noise, to add variance to the training SVG paths. Our final dataset contains 160K ⟨SVG, PVD⟩ pairs. More details can be found in Appendix C.

We fine-tune a pretrained Mistral-7b (Jiang et al., 2023) model on the synthesized PVD 160K dataset to perform SVG-to-PVD generation. We conduct full-parameter fine-tuning for 3 epochs with a learning rate of 1e-5. The training objective is a standard Language Modeling loss on the generated PVD tokens as follows:

$$\mathcal{L} = -\frac{1}{N}\sum_{i=1}^{N} \log P(\mathbf{d}_i | \mathbf{s}, \mathbf{d}_{0:i-1}) \tag{1}$$

where $\mathbf{s}$ and $\mathbf{d}$ refer to the input SVG tokens and the generated PVD tokens respectively. We use the Megatron-LLM (Cano et al., 2023) library for efficient LLM fine-tuning and the entire training process can be done in 16 hours on 4 NVIDIA A100-40GB GPUs.

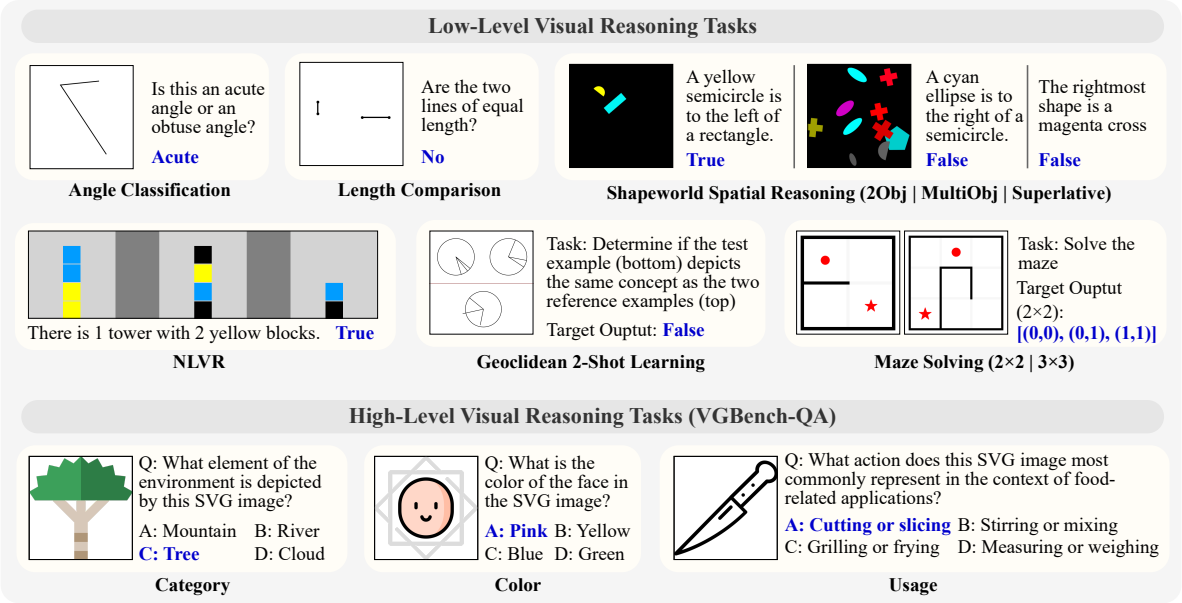

Figure 4: Our full evaluation benchmark with a focus on **low-level visual reasoning** about vector graphics (detailed in 3.1). We additionally include high-level reasoning tasks with rendered SVG images from VGBench-QA (Zou et al., 2024). All tasks are evaluated in a zero-shot setting.

2.3 Enhancing Low-Level Visual Reasoning with Primal Visual Descriptions

PVD provides precise visual details that are highly complementary to the semantic-centric visual features from pretrained visual encoders, such as CLIP. Its textual nature further facilitates direct integration into an inference-only LLM or LMM reasoner.

We explore two variants of VDLM: **VDLM-mm** and **VDLM-txt**, based on the type of reasoner applied. By default, VDLM utilizes a multimodal LMM as the reasoner, referred to as VDLM-mm, which takes both the original image and the PVD perception as input. To examine the efficacy of using PVD to represent visual information, we also consider VDLM-txt, which uses a text-only LLM as the reasoner. A detailed execution trace of the VDLM functions is illustrated in Figure 2. We observe that a strong reasoner, such as GPT-4 (OpenAI, 2023a), without any fine-tuning, can effectively perform various types of task-specific reasoning based on the PVD representation. This includes identifying higher-level concepts, computing measurements, examining spatial relations, and performing multi-step reasoning. The reasoning procedure is also more explainable and transparent compared to the output of existing monolithic LMMs.

3 Experiments

3.1 Tasks

Low-level visual reasoning tasks. Evaluating LMMs in tasks that require precise visual perception about vector graphics is a highly underexplored research area and has limited existing resources. To this end, we construct a new evaluation benchmark that comprises 9 tasks which cover important aspects of low-level visual perception and reasoning, including measurements, spatial relations, counting, logical reasoning, and complex reasoning problems such as maze solving. The description of each task is as follows: (1) **Angle Classification**: Identify whether an angle is acute or obtuse. (2) **Length Comparison**: Determine whether two line segments are of equal length. (3-4) **Shapeworld Spatial Reasoning**: The Shapeworld (Kuhnle & Copestake, 2017) dataset on spatial relations with images containing exactly two objects or multiple objects. (5) **Shapeworld Superlative**: The Shapeworld dataset on superlative statements. (6) **NLVR**: The Natural Language for Visual Reasoning dataset (Suhr et al., 2017) which contains diverse counting, spatial reasoning, and logical reasoning queries. (7) **Geoclidean 2-shot Learning**: A repurposed Geoclidean (Hsu et al.,

Low-level Visual Reasoning on Vector Graphics											
	Tools	**AC**	**LC**	**SW-S 2Obj**	**SW-S mObj**	**SW Sup**	**NLVR**	**Geo**	**Maze 2×2**	**Maze 3×3**	**All**
Monolithic Large Multimodal Models											
Llava-1.5-7b	-	0.53	0.49	0.48	0.55	0.35	0.53	0.50	0.00	0.00	0.381
Llava-1.5-13b	-	0.53	0.51	0.51	0.47	0.61	0.48	0.50	0.00	0.00	0.401
Gllava-7b	-	0.59	0.50	0.43	0.54	0.43	0.49	0.58	0.00	0.00	0.396
GPT-4V	-	0.58	0.64	0.77	0.60	0.61	0.63	0.64	0.28	0.02	0.530
GPT-4o	-	0.63	0.57	**0.97**	**0.82**	**0.92**	0.81	**0.71**	0.46	0.08	0.663
Visual Programming with LLM (text-only) reasoner											
ViperGPT (w/ GPT-4)	CI	0.11	0.67	0.61	0.47	0.53	0.43	0.02	0.03	0.00	0.319
VDLM with LLM (text-only) reasoners											
VDLM-txt (w/ GPT-4)	-	0.89	0.95	0.78	0.63	0.80	0.68	0.63	0.40	0.19	0.661
VDLM-txt (w/ GPT-4)	CI	0.73	0.95	0.89	0.68	0.72	0.72	0.64	0.40	0.26	0.666
VDLM with LMM (multimodal) reasoners											
VDLM-mm (w/ GPT-4V)	-	0.55	0.94	0.84	0.62	0.72	0.71	0.69	0.60	0.20	0.652
VDLM-mm (w/ GPT-4o)	-	**0.90**	**0.95**	0.91	**0.82**	0.82	**0.86**	**0.71**	**0.61**	**0.34**	**0.769**

Table 1: Zero-shot accuracy on low-level visual reasoning tasks. Task abbreviations: AC (Angle Classification), LC (Length Comparison), SW-S-2Obj/mObj (Shapeworld Spatial Reasoning with two objects or multiple objects), SW-Sup (Shapeworld Superlative), Geo (Geoclidean 2-shot Learning). "CI" refers to Code Interpreter. VDLM-mm brings consistent overall improvements to GPT-4V and GPT-4o, as indicated by the comparison within the blue and orange rows. Detailed analysis is presented in §3.3 and §4.

High-level Visual Reasoning on Vector Graphics				
	VGBench-QA			
	Category	**Color**	**Usage**	**All**
Llava-v1.5-7b	0.26	0.32	0.27	0.283
Llava-v1.5-13b	0.32	0.43	0.39	0.380
Gllava-7b	0.16	0.33	0.21	0.233
GPT-4o	0.58	0.84	**0.76**	0.726
VDLM-mm (w/ GPT-4o)	**0.62**	**0.86**	0.75	**0.743**

Table 2: Zero-shot accuracy on high-level visual reasoning tasks. We show that VDLM-mm preserves the LMM's capability on semantic-centric reasoning that does not require precise low-level perception.

2022) dataset requiring the model to understand a compositional geometric concept with only two reference examples. (8-9) **Maze Solving**: Solve a 2×2 or 3×3 maze, given the starting and ending positions. Among these tasks, Angle Classification, Length Comparison, and Maze Solving are newly created from scratch (See Appendix K for more details).

High-level visual reasoning tasks. Although the focus of this work is on low-level visual reasoning, we additionally include a set of high-level tasks to investigate the impact of VDLM on knowledge reasoning tasks. These tasks rarely require precise perception of the locations and measurements of the primitives. We leverage VGBench (Zou et al., 2024), a benchmark originally proposed for evaluating LLMs in understanding and generating vector graphics codes. In this work, we evaluate LMMs and VDLM-mm for question-answering based on the rasterized VGBench SVG images.

Figure 4 shows simplified input and output examples for each task. Full prompts can be found in Appendix J. To reduce the cost of evaluating proprietary models, we randomly sample a subset of 100 instances for each task. We consider a zero-shot evaluation setting for all tasks. Note that the SVG-to-PVD model in VDLM is trained purely on synthesized task-agnostic data.

3.2 Models

We compare our work with strong baselines, including both state-of-the-art monolithic large multimodal models (LMMs), i.e., LLaVA-v1.5 (Liu et al., 2023a), GLLaVA Gao et al. (2023), GPT-4V (OpenAI,

2023a)*, GPT-4o (OpenAI, 2024)†, as well as visual programming agents, e.g., ViperGPT (Surís et al., 2023). ViperGPT employs an LLM to generate code, which can call external vision models, such as GLIP (Li et al., 2022) and BLIP2 (Li et al., 2023b), to process the image and generate the final output. Given that ViperGPT-style models successfully separate perception from reasoning, we seek to investigate whether the existing perception tools adequately recognize low-level primitives in vector graphics. For VDLM, we explore two variants, namely VDLM-mm with GPT-4V, GPT-4o and VDLM-txt with GPT-4 (text-only). ‡ We also experiment with applying weaker LMM reasoners, such as LLaVA, to VDLM-mm. We find that interpreting PVD requires a certain level of text reasoning capability, and the benefits only emerge with strong LMMs, as shown in Figure 5. However, recent strong open-source LMMs, such as Qwen-2.5-VL-72B (Bai et al., 2025), can also benefit from PVD features (see Appendix F for additional experiments). To obtain more insights in comparing with ViperGPT, we further investigate augmenting VDLM-txt with a Code Interpreter (CI). We employ the GPT-4 Assistant § for our experiments, designating the code interpreter as the sole tool available. We use the same set of prompts for both VDLM-txt and VDLM-mm. See details about prompt design in Appendix J.

3.3 Results

Table 1 shows the zero-shot accuracy for the evaluation tasks. We outline the key findings as follows:

VDLM significantly improves LMMs on low-level reasoning tasks, while preserving their capabilities in high-level reasoning. The fact that VDLM-txt performs competitively even with a text-only reasoner highlights the efficacy of the intermediate PVD representation for precise low-level visual perception. Without any task-specific fine-tuning, strong LMM reasoners can effectively incorporate the additional information provided PVD alongside the image input. Figure 5 further demonstrates that this benefit only emerges when the LMM has a certain level of text-reasoning ability and persists in state-of-the-art LMMs. For high-level reasoning tasks (Table 2), the improvement is more subtle, as the tasks focus on the semantics of the vector graphics, such as "what can this be used for?", which rarely require precise location or measurements of visual elements.

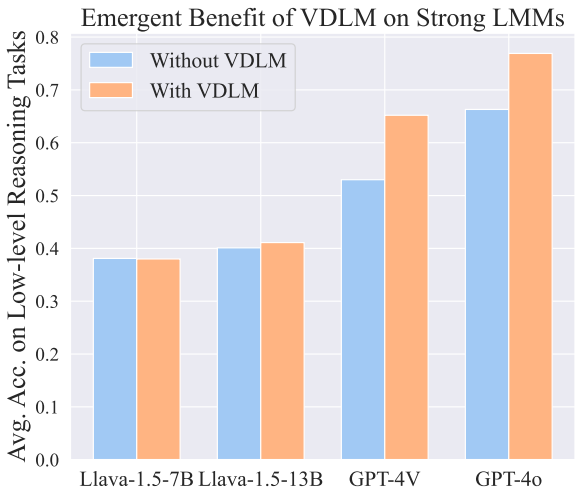

Figure 5: The direct improvements brought by VDLM to LMMs emerge when the LMM possesses sufficient text reasoning capabilities. These improvements are consistent with stronger LMMs, such as GPT-4o, which have enhanced spatial reasoning performance.

QA performance on complex math problems does not necessarily reflect a faithful understanding of low-level visual concepts. We observe that G-LLaVA (Gao et al., 2023), a model demonstrating strong performance on geometric problems, such as MathVista (Lu et al., 2023), still struggles with understanding basic lines and angles, which are prerequisites for solving geometric math problems.

Existing vision-language models, such as GLIP and BLIP2, are ineffective as low-level visual preceptors. This is evidenced by the unsatisfactory performance of ViperGPT, even when equipped with a strong planner like GPT-4. On the other hand, we observe that augmenting the reasoning model in VDLM-txt with code interpreters can be particularly helpful for tasks requiring algorithmic reasoning, such as 3×3 maze solving.

*GPT-4V model version: gpt-4-1106-vision-preview.
†GPT-4o model version: gpt-4o-2024-05-13
‡GPT-4 (text-only) model version: gpt-4-0125-preview.
§`https://platform.openai.com/docs/assistants/overview/agents`

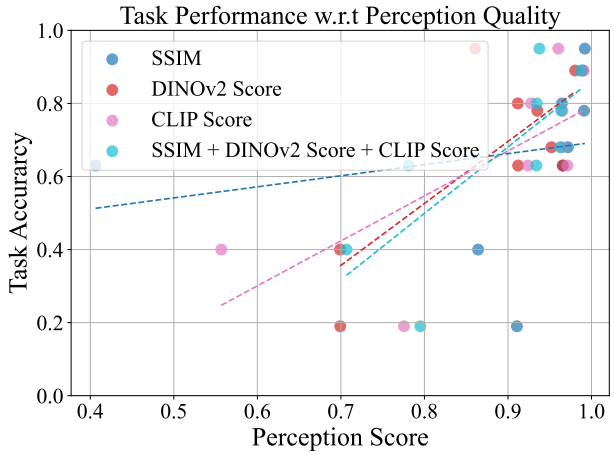

Figure 6: Task-level correlation between PVD perception quality and end-task performance.

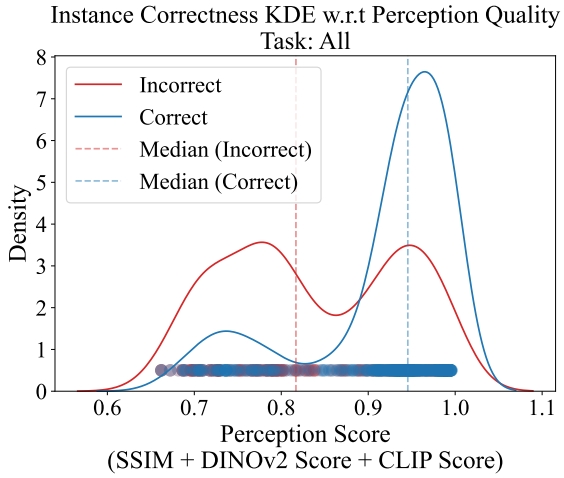

Figure 7: Instance-level correlation between PVD perception quality and end-task performance. We observe a consistent positive correlation as in task-level.

Impact of errors in PVD perception. In certain tasks, such as Shapeworld Spatial Reasoning, GPT-4o achieves better performance than VDLM-mm. The reason lies in the imperfect perception results of the SVG-to-PVD model, despite the image-to-SVG step achieving near-perfect reconstruction as shown in Appendix D. Since the SVG-to-PVD model is trained with purely synthetic data, it is not yet perfect when generalizing to diverse domains. In Appendix E, we present an additional ablation study on the design choices of the PVD model, including alternative LLM selections and a comparison to the PNG-to-PVD approach. We also carefully analyze the remaining errors in §4.2, and demonstrate the impact of improving perception on end-task performance (§4.1). In §6, we discuss future work for developing a more general and expressive PVD representation.

4 Analysis

4.1 Primal Visual Description Quality vs End-Task Performance

One advantage of a modular system is that enhancing an individual module can leads to improvements in the overall system. In this section, we explore whether a positive correlation exists between the quality of the intermediate perception representation and end-task performance. To investigate this, we first define metrics to reflect the quality of the PVD perception. Upon generating a PVD perception result, we render it back into a raster image using our procedural image generator. We then compute a similarity score between the reconstructed image and the original input image as a measure of the perception performance. For measuring the similarity, we consider both pixel-based and embedding-based metrics. We adopt the Structural Similarity (SSIM) Index (Wang et al., 2004) score to assess pixel-level similarity. Additionally, to account for semantic similarity, we adopt a CLIP-score (Radford et al., 2021) and a DINOv2-score (Oquab et al., 2023), which are calculated as the cosine similarity of the flattened CLIP and DINOv2 embeddings, respectively.

In Figures 6 and 7, we visualize the impact of the perception quality, on the 9 low-level reasoning tasks with VDLM-txt, at both the task and instance levels. In Figure 6, each point denotes the accuracy of a task, with different colors representing different similarity metrics. The dashed lines depict linear regression results of the points, revealing a consistent positive correlation between perception quality and task accuracy across the metrics. Since the task-level accuracy may not be directly comparable across different tasks, we additionally perform an instance-level analysis using Kernel Density Estimation (KDE) on the correctness of all task instances with respect to their perception scores. As shown in Figure 7, the "correct" distribution visibly skews to the area of higher perception scores, indicating that better perception tends to result in a correct

final answer. This finding is promising, suggesting that enhancing the intermediate PVD representation, even with a fixed reasoning model, can effectively boost downstream task performance.

4.2 Interpretable Error Analysis

The improved interpretability, resulting from PVD's disentangled perception and reasoning, allows us to conduct an in-depth analysis of the failure modes of VDLM. We find that both the perception step (SVG-to-PVD) and the reasoning step (PVD-to-answer) can contribute to errors. On tasks that require complex multistep reasoning, such as Maze Solving, reasoning errors become more prevalent; otherwise, perception errors most directly contribute to poor performance. Details and illustrative examples of these errors are provided in **Appendix B**, along with a distribution of perception and reasoning errors from human analyses. The prevalent error types for both perception and reasoning steps are summarized as follows.

Common perception errors include failures in faithfully perceiving novel shapes that are not covered by or cannot be composed within the PVD ontology, and failures in capturing intentional constraints between primitives, such as a line exactly segmenting a circle, due to the random nature of the data generation on the positioning of objects. In Table 5, we show that the proposed augmentation during synthetic data generation improves PVD perception. Common reasoning errors over the PVD perception include failures in discovering intentional constraints without being explicitly asked, such as automatically recognizing that a rhombus is not the same concept as a general quadrilateral; failure in handling ambiguous instructions; and failure in complex multi-step reasoning tasks like solving mazes.

5 Related Work

Visual shortcomings in large multimodal models. While state-of-the-art LMMs achieve strong performance on existing multimodal benchmarks (Goyal et al., 2017; Fu et al., 2023; Liu et al., 2023b;d; Yu et al., 2023; Li et al., 2023a), which primarily focus on natural images, recent work (Lu et al., 2023; Yue et al., 2023; Huang et al., 2023; Zhou et al., 2023a; Hsu et al., 2022; Gao et al., 2023) has shown that they struggle with charts, geometric diagrams, and abstract scenes. This observation aligns with recent studies investigating visual shortcomings in LMMs. Tong et al. (2024) suggests that current LMMs struggle with visual details because the image-text contrastive pretraining of the CLIP visual backbone does not encourage the preservation of fine-grained visual features, such as orientation and quantity. To address this issue, recent studies have either leveraged the mixture-of-experts approach (Tong et al., 2024; Fan et al., 2024; Lu et al., 2024; Jain et al., 2023b), incorporating various types of vision encoders, such as SAM (Kirillov et al., 2023), DINOv2 (Oquab et al., 2023), or introduced auxiliary losses that emphasize local details during multimodal pretraining McKinzie et al. (2024); Bica et al. (2024); Varma et al. (2023). In this work, we propose a novel perspective for addressing this visual deficiency in vector graphics with an intermediate perception representation.

Image vectorization and program synthesis. Generating vectorized or symbolic representations of visual concepts has been a topic of interest in both the NLP and computer vision communities. Recent work (Vinker et al., 2022; Lee et al., 2023; Ma et al., 2022; Rodriguez et al., 2023; Jain et al., 2023a; Tang et al., 2024; Xing et al., 2024; Hu et al., 2024) has investigated generating vector graphics codes from raster images or text prompts. We focus on the reverse problem of understanding and reasoning about vector graphics as visual inputs. We find that vector graphics reasoning serves as a challenging testbed to evaluate low-level visual reasoning abilities in large multimodal models (LMMs). Although Bubeck et al. (2023); Cai et al. (2023); Zou et al. (2024); Qiu et al. (2024) have demonstrated the potential of text-only large language models (LLMs) in understanding the semantics of vector graphics codes, it remains unclear how to enhance the ability of large *multimodal* models to process *rasterized* vector graphics without access to the underlying code, which is more common in real-world scenarios. Therefore, we propose the intermediate Primal Visual Description representation to further enhance low-level perception and reasoning, without sacrificing the performance of semantic understanding. This work is also heavily inspired by related work in neural-symbolic models (Ritchie et al., 2016; Wu et al., 2017; Yi et al., 2018; Mao et al., 2019; Hsu et al., 2023; Zhang et al., 2023; Trinh et al., 2024). This paradigm aims to de-render visual scenes into structured representations, retrieve programs from the input text, and execute these programs on the image representations. However,

most neural-symbolic work can not be applied to recent LMMs and is limited to specific tasks. We aim to learn a task-agnostic visual description that can be directly reasoned about by off-the-shelf LMMs.

Disentangling perception and reasoning in large multimodal models. Another closely related line of work has investigated disentangling visual perception and reasoning with visual programming (Gupta & Kembhavi, 2023; Surís et al., 2023; Ge et al., 2023; Wu & Xie, 2023) and tool-using (Wu et al., 2023; Liu et al., 2023c; Qiao et al., 2024). These models leverage the code generation capabilities of LLMs to compose and employ a set of vision-language or vision-only models, such as object detection and image caption models, as subroutines for solving visual reasoning tasks. Despite promising performance on natural images, as shown in § 3, we find that these models are still limited by the existing vision-language models' inability to process low-level primitives effectively.

6 Limitations and Future Work

VDLM represents an initial step to constructing a descriptive intermediate representation for low-level visual reasoning. While our results strongly support this proof of concept, several limitations remain, highlighting directions for future work.

First, due to the scarcity of end-to-end instructional tuning data (discussed in §2.1), the current SVG-to-PVD model is constrained to compositions of simple primitives, for which we can synthesize data without requiring annotation. To enhance PVD's generalization across more diverse domains, we identify several possible improvements. For instance, incorporating human-created vector graphics with procedural annotations could enrich the ontology and training dataset. Additionally, integrating visual search Wu & Xie (2023) during inference could facilitate the conversion of focused regions or parts into PVD, enabling multi-step perception and reasoning. Second, SVG and PVD are inherently designed for representing 2D vector graphics. Future research is needed to develop a more general intermediate representation that extends beyond 2D vector graphics to encompass 3D structures and natural images.

Acknowledgments

This research is based upon work supported by U.S. DARPA ECOLE Program No. #HR00112390060, AFOSR YIP FA9550-23-1-0127, ONR N00014-23-1-2355, ONR YIP N00014-24-1-2117, ONR MURI N00014-24-1-2748, and the Stanford Institute for Human-Centered AI (HAI). The views and conclusions contained herein are those of the authors and should not be interpreted as necessarily representing the official policies, either expressed or implied, of DARPA, or the U.S. Government. The U.S. Government is authorized to reproduce and distribute reprints for governmental purposes notwithstanding any copyright annotation therein.

References

Rohan Anil, Sebastian Borgeaud, Yonghui Wu, Jean-Baptiste Alayrac, Jiahui Yu, Radu Soricut, Johan Schalkwyk, Andrew M. Dai, Anja Hauth, Katie Millican, David Silver, Slav Petrov, Melvin Johnson, Ioannis Antonoglou, Julian Schrittwieser, Amelia Glaese, Jilin Chen, Emily Pitler, Timothy P. Lillicrap, Angeliki Lazaridou, Orhan Firat, James Molloy, Michael Isard, Paul Ronald Barham, Tom Hennigan, Benjamin Lee, Fabio Viola, Malcolm Reynolds, Yuanzhong Xu, Ryan Doherty, Eli Collins, Clemens Meyer, Eliza Rutherford, Erica Moreira, Kareem Ayoub, Megha Goel, George Tucker, Enrique Piqueras, Maxim Krikun, Iain Barr, Nikolay Savinov, Ivo Danihelka, Becca Roelofs, Anaïs White, Anders Andreassen, Tamara von Glehn, Lakshman Yagati, Mehran Kazemi, Lucas Gonzalez, Misha Khalman, Jakub Sygnowski, and et al. Gemini: A Family of Highly Capable Multimodal Models. *arXiv prepring arXiv:2312.11805*, 2023. URL `https://doi.org/10.48550/arXiv.2312.11805`.

Jinze Bai, Shuai Bai, Shusheng Yang, Shijie Wang, Sinan Tan, Peng Wang, Junyang Lin, Chang Zhou, and Jingren Zhou. Qwen-VL: A Frontier Large Vision-Language Model with Versatile Abilities. *arXiv preprint arXiv:2308.12966*, 2023. URL `https://doi.org/10.48550/arXiv.2308.12966`.

Shuai Bai, Keqin Chen, Xuejing Liu, Jialin Wang, Wenbin Ge, Sibo Song, Kai Dang, Peng Wang, Shijie Wang, Jun Tang, et al. Qwen2. 5-vl technical report. *arXiv preprint arXiv:2502.13923*, 2025.

Ioana Bica, Anastasija Ilic, Matthias Bauer, Goker Erdogan, Matko Bosnjak, Christos Kaplanis, Alexey A. Gritsenko, Matthias Minderer, Charles Blundell, Razvan Pascanu, and Jovana Mitrovic. Improving Fine-Grained Understanding in Image-Text Pre-Training. *arXiv prepring arXiv:2401.09865*, 2024. URL https://doi.org/10.48550/arXiv.2401.09865.

Sébastien Bubeck, Varun Chandrasekaran, Ronen Eldan, Johannes Gehrke, Eric Horvitz, Ece Kamar, Peter Lee, Yin Tat Lee, Yuanzhi Li, Scott M. Lundberg, Harsha Nori, Hamid Palangi, Marco Túlio Ribeiro, and Yi Zhang. Sparks of Artificial General Intelligence: Early Experiments with GPT-4. *arXiv prepring arXiv:2303.12712*, 2023. URL https://doi.org/10.48550/arXiv.2303.12712.

Mu Cai, Zeyi Huang, Yuheng Li, Haohan Wang, and Yong Jae Lee. Leveraging Large Language Models for Scalable Vector Graphics-Driven Image Understanding. *arXiv prepring arXiv:2306.06094*, 2023. URL https://doi.org/10.48550/arXiv.2306.06094.

Alejandro Hernández Cano, Matteo Pagliardini, Andreas Köpf, Kyle Matoba, Amirkeivan Mohtashami, Xingyao Wang, Olivia Simin Fan, Axel Marmet, Deniz Bayazit, Igor Krawczuk, Zeming Chen, Francesco Salvi, Antoine Bosselut, and Martin Jaggi. EpfLLM Megatron-LLM, 2023. URL https://github.com/epfLLM/Megatron-LLM.

Lin Chen, Jinsong Li, Xiaoyi Dong, Pan Zhang, Conghui He, Jiaqi Wang, Feng Zhao, and Dahua Lin. ShareGPT4V: Improving Large Multi-Modal Models with Better Captions, 2023a. URL https://doi.org/10.48550/arXiv.2311.12793.

Zhe Chen, Jiannan Wu, Wenhai Wang, Weijie Su, Guo Chen, Sen Xing, Muyan Zhong, Qinglong Zhang, Xizhou Zhu, Lewei Lu, Bin Li, Ping Luo, Tong Lu, Yu Qiao, and Jifeng Dai. InternVL: Scaling up Vision Foundation Models and Aligning for Generic Visual-Linguistic Tasks. *arXiv prepring arXiv:2312.14238*, 2023b. URL https://doi.org/10.48550/arXiv.2312.14238.

Wei-Lin Chiang, Zhuohan Li, Zi Lin, Ying Sheng, Zhanghao Wu, Hao Zhang, Lianmin Zheng, Siyuan Zhuang, Yonghao Zhuang, Joseph E. Gonzalez, Ion Stoica, and Eric P. Xing. Vicuna: An Open-Source Chatbot Impressing GPT-4 with 90%* ChatGPT Quality, March 2023. URL https://lmsys.org/blog/2023-03-30-vicuna/.

Wenliang Dai, Junnan Li, Dongxu Li, Anthony Meng Huat Tiong, Junqi Zhao, Weisheng Wang, Boyang Li, Pascale Fung, and Steven C. H. Hoi. InstructBLIP: Towards General-purpose Vision-Language Models with Instruction Tuning. In *Advances in Neural Information Processing Systems 36: Annual Conference on Neural Information Processing Systems 2023 (NeurIPS)*, 2023. URL http://papers.nips.cc/paper_files/paper/2023/hash/9a6a435e75419a836fe47ab6793623e6-Abstract-Conference.html.

Xiaoran Fan, Tao Ji, Changhao Jiang, Shuo Li, Senjie Jin, Sirui Song, Junke Wang, Boyang Hong, Lu Chen, Guodong Zheng, Ming Zhang, Caishuang Huang, Rui Zheng, Zhiheng Xi, Yuhao Zhou, Shihan Dou, Junjie Ye, Hang Yan, Tao Gui, Qi Zhang, Xipeng Qiu, Xuanjing Huang, Zuxuan Wu, and Yu-Gang Jiang. MouSi: Poly-Visual-Expert Vision-Language Models. *arXiv prepring arXiv:2401.17221*, 2024. URL https://doi.org/10.48550/arXiv.2401.17221.

Chaoyou Fu, Peixian Chen, Yunhang Shen, Yulei Qin, Mengdan Zhang, Xu Lin, Zhenyu Qiu, Wei Lin, Jinrui Yang, Xiawu Zheng, Ke Li, Xing Sun, and Rongrong Ji. MME: A Comprehensive Evaluation Benchmark for Multimodal Large Language Models. *arXiv prepring arXiv:2306.13394*, 2023. URL https://doi.org/10.48550/arXiv.2306.13394.

Jiahui Gao, Renjie Pi, Jipeng Zhang, Jiacheng Ye, Wanjun Zhong, Yufei Wang, Lanqing Hong, Jianhua Han, Hang Xu, Zhenguo Li, and Lingpeng Kong. G-LLaVA: Solving Geometric Problem with Multi-Modal Large Language Model. *arXiv prepring arXiv:2312.11370*, 2023. URL https://doi.org/10.48550/arXiv.2312.11370.

Jiaxin Ge, Sanjay Subramanian, Baifeng Shi, Roei Herzig, and Trevor Darrell. Recursive Visual Programming. *arXiv prepring arXiv:2312.02249*, 2023. URL https://doi.org/10.48550/arXiv.2312.02249.

Yash Goyal, Tejas Khot, Douglas Summers-Stay, Dhruv Batra, and Devi Parikh. Making the V in VQA Matter: Elevating the Role of Image Understanding in Visual Question Answering. In *2017 IEEE Conference on Computer Vision and Pattern Recognition (CVPR)*, 2017. URL https://doi.org/10.1109/CVPR.2017.670.

Tanmay Gupta and Aniruddha Kembhavi. Visual Programming: Compositional Visual Reasoning without Training. In *IEEE/CVF Conference on Computer Vision and Pattern Recognition (CVPR)*, 2023. URL https://doi.org/10.1109/CVPR52729.2023.01436.

Joy Hsu, Jiajun Wu, and Noah D. Goodman. Geoclidean: Few-Shot Generalization in Euclidean Geometry. In *Advances in Neural Information Processing Systems 35: Annual Conference on Neural Information Processing Systems 2022 (NeurIPS)*, 2022. URL http://papers.nips.cc/paper_files/paper/2022/hash/feb34ce77fc8b94c85d12e608b23ce67-Abstract-Datasets_and_Benchmarks.html.

Joy Hsu, Jiayuan Mao, Joshua B. Tenenbaum, and Jiajun Wu. What's Left? Concept Grounding with Logic-Enhanced Foundation Models. In *Advances in Neural Information Processing Systems 36: Annual Conference on Neural Information Processing Systems 2023 (NeurIPS)*, 2023. URL http://papers.nips.cc/paper_files/paper/2023/hash/79fea214543ba263952ac3f4e5452b14-Abstract-Conference.html.

Edward J. Hu, Yelong Shen, Phillip Wallis, Zeyuan Allen-Zhu, Yuanzhi Li, Shean Wang, Lu Wang, and Weizhu Chen. LoRA: Low-Rank Adaptation of Large Language Models. In *The Tenth International Conference on Learning Representations (ICLR)*, 2022. URL https://openreview.net/forum?id=nZeVKeeFYf9.

Juncheng Hu, Ximing Xing, Zhengqi Zhang, Jing Zhang, and Qian Yu. Vectorpainter: A novel approach to stylized vector graphics synthesis with vectorized strokes. *arXiv preprint arXiv:2405.02962*, 2024.

Kung-Hsiang Huang, Mingyang Zhou, Hou Pong Chan, Yi R. Fung, Zhenhailong Wang, Lingyu Zhang, Shih-Fu Chang, and Heng Ji. Do LVLMs Understand Charts? Analyzing and Correcting Factual Errors in Chart Captioning. *arXiv prepring arXiv:2312.10160*, 2023. URL https://doi.org/10.48550/arXiv.2312.10160.

Ajay Jain, Amber Xie, and Pieter Abbeel. VectorFusion: Text-to-SVG by Abstracting Pixel-Based Diffusion Models. In *IEEE/CVF Conference on Computer Vision and Pattern Recognition (CVPR)*, 2023a. URL https://doi.org/10.1109/CVPR52729.2023.00190.

Jitesh Jain, Jianwei Yang, and Humphrey Shi. VCoder: Versatile Vision Encoders for Multimodal Large Language Models. *arXiv prepring arXiv:2312.14233*, 2023b. URL https://doi.org/10.48550/arXiv.2312.14233.

Albert Q. Jiang, Alexandre Sablayrolles, Arthur Mensch, Chris Bamford, Devendra Singh Chaplot, Diego de Las Casas, Florian Bressand, Gianna Lengyel, Guillaume Lample, Lucile Saulnier, Lélio Renard Lavaud, Marie-Anne Lachaux, Pierre Stock, Teven Le Scao, Thibaut Lavril, Thomas Wang, Timothée Lacroix, and William El Sayed. Mistral 7B. *arXiv prepring arXiv:2310.06825*, 2023. URL https://doi.org/10.48550/arXiv.2310.06825.

Alexander Kirillov, Eric Mintun, Nikhila Ravi, Hanzi Mao, Chloé Rolland, Laura Gustafson, Tete Xiao, Spencer Whitehead, Alexander C. Berg, Wan-Yen Lo, Piotr Dollár, and Ross B. Girshick. Segment Anything. In *IEEE/CVF International Conference on Computer Vision (ICCV)*, 2023. URL https://doi.org/10.1109/ICCV51070.2023.00371.

Ranjay Krishna, Yuke Zhu, Oliver Groth, Justin Johnson, Kenji Hata, Joshua Kravitz, Stephanie Chen, Yannis Kalantidis, Li-Jia Li, David A. Shamma, Michael S. Bernstein, and Li Fei-Fei. Visual Genome: Connecting Language and Vision Using Crowdsourced Dense Image Annotations. *Int. J. Comput. Vis.*, 123(1):32–73, 2017. URL https://doi.org/10.1007/s11263-016-0981-7.

Benno Krojer, Vaibhav Adlakha, Vibhav Vineet, Yash Goyal, Edoardo Maria Ponti, and Siva Reddy. Image Retrieval from Contextual Descriptions. In *Proceedings of the 60th Annual Meeting of the Association for Computational Linguistics (ACL)*, 2022. URL https://doi.org/10.18653/v1/2022.acl-long.241.

Joseph B Kruskal. On the Shortest Spanning Subtree of a Graph and the Traveling Salesman Problem. *Proceedings of the American Mathematical society*, 7(1):48–50, 1956.

Alexander Kuhnle and Ann A. Copestake. ShapeWorld - A New Test Methodology for Multimodal Language Understanding. *arXiv prepring arXiv:1704.04517*, 2017. URL http://arxiv.org/abs/1704.04517.

Hyundo Lee, Inwoo Hwang, Hyunsung Go, Won-Seok Choi, Kibeom Kim, and Byoung-Tak Zhang. Learning Geometry-Aware Representations by Sketching. In *IEEE/CVF Conference on Computer Vision and Pattern Recognition (CVPR)*, 2023. URL https://doi.org/10.1109/CVPR52729.2023.02233.

Bohao Li, Rui Wang, Guangzhi Wang, Yuying Ge, Yixiao Ge, and Ying Shan. SEED-Bench: Benchmarking Multimodal LLMs with Generative Comprehension. *arXiv prepring arXiv:2307.16125*, 2023a. URL https://doi.org/10.48550/arXiv.2307.16125.

Junnan Li, Dongxu Li, Silvio Savarese, and Steven C. H. Hoi. BLIP-2: Bootstrapping Language-Image Pre-training with Frozen Image Encoders and Large Language Models. In *International Conference on Machine Learning (ICML)*, 2023b. URL https://proceedings.mlr.press/v202/li23q.html.

Liunian Harold Li, Pengchuan Zhang, Haotian Zhang, Jianwei Yang, Chunyuan Li, Yiwu Zhong, Lijuan Wang, Lu Yuan, Lei Zhang, Jenq-Neng Hwang, Kai-Wei Chang, and Jianfeng Gao. Grounded Language-Image Pre-training. In *IEEE/CVF Conference on Computer Vision and Pattern Recognition (CVPR)*, 2022. URL https://doi.org/10.1109/CVPR52688.2022.01069.

Tsung-Yi Lin, Michael Maire, Serge J. Belongie, James Hays, Pietro Perona, Deva Ramanan, Piotr Dollár, and C. Lawrence Zitnick. Microsoft COCO: Common Objects in Context. In *Computer Vision - ECCV 2014 - 13th European Conference*, 2014. URL https://doi.org/10.1007/978-3-319-10602-1_48.

Haotian Liu, Chunyuan Li, Yuheng Li, and Yong Jae Lee. Improved Baselines with Visual Instruction Tuning. *arXiv prepring arXiv:2310.03744*, 2023a. URL https://doi.org/10.48550/arXiv.2310.03744.

Haotian Liu, Chunyuan Li, Qingyang Wu, and Yong Jae Lee. Visual Instruction Tuning. In *Advances in Neural Information Processing Systems 36: Annual Conference on Neural Information Processing Systems 2023 (NeurIPS)*, 2023b. URL http://papers.nips.cc/paper_files/paper/2023/hash/6dcf277ea32ce3288914faf369fe6de0-Abstract-Conference.html.

Shilong Liu, Hao Cheng, Haotian Liu, Hao Zhang, Feng Li, Tianhe Ren, Xueyan Zou, Jianwei Yang, Hang Su, Jun Zhu, Lei Zhang, Jianfeng Gao, and Chunyuan Li. LLaVA-Plus: Learning to Use Tools for Creating Multimodal Agents. *arXiv prepring arXiv:2311.05437*, 2023c. URL https://doi.org/10.48550/arXiv.2311.05437.

Xiao Liu, Tianjie Zhang, Yu Gu, Iat Long Iong, Yifan Xu, Xixuan Song, Shudan Zhang, Hanyu Lai, Xinyi Liu, Hanlin Zhao, et al. Visualagentbench: Towards large multimodal models as visual foundation agents. *arXiv preprint arXiv:2408.06327*, 2024.

Yuan Liu, Haodong Duan, Yuanhan Zhang, Bo Li, Songyang Zhang, Wangbo Zhao, Yike Yuan, Jiaqi Wang, Conghui He, Ziwei Liu, Kai Chen, and Dahua Lin. MMBench: Is Your Multi-modal Model an All-around Player? *arXiv prepring arXiv:2307.06281*, 2023d. URL https://doi.org/10.48550/arXiv.2307.06281.

Haoyu Lu, Wen Liu, Bo Zhang, Bingxuan Wang, Kai Dong, Bo Liu, Jingxiang Sun, Tongzheng Ren, Zhuoshu Li, Hao Yang, Yaofeng Sun, Chengqi Deng, Hanwei Xu, Zhenda Xie, and Chong Ruan. DeepSeek-VL: Towards Real-World Vision-Language Understanding. *arXiv prepring arXiv:2403.05525*, 2024. URL https://doi.org/10.48550/arXiv.2403.05525.

Pan Lu, Hritik Bansal, Tony Xia, Jiacheng Liu, Chunyuan Li, Hannaneh Hajishirzi, Hao Cheng, Kai-Wei Chang, Michel Galley, and Jianfeng Gao. MathVista: Evaluating Math Reasoning in Visual Contexts with GPT-4V, Bard, and Other Large Multimodal Models. *arXiv prepring arXiv:2310.02255*, 2023. URL https://doi.org/10.48550/arXiv.2310.02255.

Xing Han Lù, Zdeněk Kasner, and Siva Reddy. Weblinx: Real-world website navigation with multi-turn dialogue. *arXiv preprint arXiv:2402.05930*, 2024.

Xu Ma, Yuqian Zhou, Xingqian Xu, Bin Sun, Valerii Filev, Nikita Orlov, Yun Fu, and Humphrey Shi. Towards Layer-wise Image Vectorization. In *IEEE/CVF Conference on Computer Vision and Pattern Recognition (CVPR)*, 2022. URL https://doi.org/10.1109/CVPR52688.2022.01583.

Jiayuan Mao, Chuang Gan, Pushmeet Kohli, Joshua B. Tenenbaum, and Jiajun Wu. The Neuro-Symbolic Concept Learner: Interpreting Scenes, Words, and Sentences From Natural Supervision. In *7th International Conference on Learning Representations (ICLR)*, 2019. URL https://openreview.net/forum?id=rJgMlhRctm.

Kenneth Marino, Mohammad Rastegari, Ali Farhadi, and Roozbeh Mottaghi. OK-VQA: A Visual Question Answering Benchmark Requiring External Knowledge. In *IEEE Conference on Computer Vision and Pattern Recognition (CVPR)*, 2019. URL http://openaccess.thecvf.com/content_CVPR_2019/html/Marino_OK-VQA_A_Visual_Question_Answering_Benchmark_Requiring_External_Knowledge_CVPR_2019_paper.html.

Brandon McKinzie, Zhe Gan, Jean-Philippe Fauconnier, Sam Dodge, Bowen Zhang, Philipp Dufter, Dhruti Shah, Xianzhi Du, Futang Peng, Floris Weers, Anton Belyi, Haotian Zhang, Karanjeet Singh, Doug Kang, Ankur Jain, Hongyu Hè, Max Schwarzer, Tom Gunter, Xiang Kong, Aonan Zhang, Jianyu Wang, Chong Wang, Nan Du, Tao Lei, Sam Wiseman, Guoli Yin, Mark Lee, Zirui Wang, Ruoming Pang, Peter Grasch, Alexander Toshev, and Yinfei Yang. MM1: Methods, Analysis & Insights from Multimodal LLM Pre-training. *arXiv preprint arXiv:2403.09611*, 2024. URL https://doi.org/10.48550/arXiv.2403.09611.

OpenAI. GPT-4 Technical Report, 2023a.

OpenAI. GPT-4V(ision) System Card, 2023b. URL https://cdn.openai.com/papers/GPTV_System_Card.pdf.

OpenAI. GPT-4o System Card, 2024. URL https://cdn.openai.com/gpt-4o-system-card.pdf.

Maxime Oquab, Timothée Darcet, Théo Moutakanni, Huy Vo, Marc Szafraniec, Vasil Khalidov, Pierre Fernandez, Daniel Haziza, Francisco Massa, Alaaeldin El-Nouby, Mahmoud Assran, Nicolas Ballas, Wojciech Galuba, Russell Howes, Po-Yao Huang, Shang-Wen Li, Ishan Misra, Michael G. Rabbat, Vasu Sharma, Gabriel Synnaeve, Hu Xu, Hervé Jégou, Julien Mairal, Patrick Labatut, Armand Joulin, and Piotr Bojanowski. DINOv2: Learning Robust Visual Features without Supervision. *arXiv prepring arXiv:2304.07193*, 2023. URL https://doi.org/10.48550/arXiv.2304.07193.

Yuxuan Qiao, Haodong Duan, Xinyu Fang, Junming Yang, Lin Chen, Songyang Zhang, Jiaqi Wang, Dahua Lin, and Kai Chen. Prism: A framework for decoupling and assessing the capabilities of vlms. *arXiv preprint arXiv:2406.14544*, 2024.

Zeju Qiu, Weiyang Liu, Haiwen Feng, Zhen Liu, Tim Z Xiao, Katherine M Collins, Joshua B Tenenbaum, Adrian Weller, Michael J Black, and Bernhard Schölkopf. Can large language models understand symbolic graphics programs? *arXiv preprint arXiv:2408.08313*, 2024.

Alec Radford, Jong Wook Kim, Chris Hallacy, Aditya Ramesh, Gabriel Goh, Sandhini Agarwal, Girish Sastry, Amanda Askell, Pamela Mishkin, Jack Clark, Gretchen Krueger, and Ilya Sutskever. Learning Transferable Visual Models From Natural Language Supervision. In *Proceedings of the 38th International Conference on Machine Learning (ICML)*, 2021. URL http://proceedings.mlr.press/v139/radford21a.html.

Christopher Rawles, Sarah Clinckemaillie, Yifan Chang, Jonathan Waltz, Gabrielle Lau, Marybeth Fair, Alice Li, William Bishop, Wei Li, Folawiyo Campbell-Ajala, et al. Androidworld: A dynamic benchmarking environment for autonomous agents. *arXiv preprint arXiv:2405.14573*, 2024.

Daniel Ritchie, Anna Thomas, Pat Hanrahan, and Noah D. Goodman. Neurally-Guided Procedural Models: Amortized Inference for Procedural Graphics Programs using Neural Networks. In *Advances in Neural Information Processing Systems 29: Annual Conference on Neural Information Processing Systems 2016 (NeurIPS)*, 2016. URL https://proceedings.neurips.cc/paper/2016/hash/40008b9a5380fcacce3976bf7c08af5b-Abstract.html.

Juan A Rodriguez, Shubham Agarwal, Issam H Laradji, Pau Rodriguez, David Vazquez, Christopher Pal, and Marco Pedersoli. StarVector: Generating Scalable Vector Graphics Code from Images. *arXiv preprint arXiv:2312.11556*, 2023.

Dustin Schwenk, Apoorv Khandelwal, Christopher Clark, Kenneth Marino, and Roozbeh Mottaghi. A-OKVQA: A Benchmark for Visual Question Answering Using World Knowledge. In *Computer Vision - ECCV 2022 - 17th European Conference*, 2022. URL https://doi.org/10.1007/978-3-031-20074-8_9.

Oleksii Sidorov, Ronghang Hu, Marcus Rohrbach, and Amanpreet Singh. TextCaps: A Dataset for Image Captioning with Reading Comprehension. In *Computer Vision - ECCV 2020 - 16th European Conference*, 2020. URL https://doi.org/10.1007/978-3-030-58536-5_44.

Alane Suhr, Mike Lewis, James Yeh, and Yoav Artzi. A Corpus of Natural Language for Visual Reasoning. In *Proceedings of the 55th Annual Meeting of the Association for Computational Linguistics (ACL)*, 2017. URL https://doi.org/10.18653/v1/P17-2034.

Dídac Surís, Sachit Menon, and Carl Vondrick. ViperGPT: Visual Inference via Python Execution for Reasoning. In *IEEE/CVF International Conference on Computer Vision (ICCV)*, 2023. URL https://doi.org/10.1109/ICCV51070.2023.01092.

Zecheng Tang, Chenfei Wu, Zekai Zhang, Mingheng Ni, Shengming Yin, Yu Liu, Zhengyuan Yang, Lijuan Wang, Zicheng Liu, Juntao Li, et al. Strokenuwa: Tokenizing strokes for vector graphic synthesis. *arXiv preprint arXiv:2401.17093*, 2024.

Shengbang Tong, Zhuang Liu, Yuexiang Zhai, Yi Ma, Yann LeCun, and Saining Xie. Eyes Wide Shut? Exploring the Visual Shortcomings of Multimodal LLMs. *arXiv prepring arXiv:2401.06209*, 2024. URL https://doi.org/10.48550/arXiv.2401.06209.

Trieu H. Trinh, Yuhuai Wu, Quoc V. Le, He He, and Thang Luong. Solving Olympiad Geometry without Human Demonstrations. *Nat.*, 625(7995):476–482, 2024. URL https://doi.org/10.1038/s41586-023-06747-5.

Maya Varma, Jean-Benoit Delbrouck, Sarah M. Hooper, Akshay Chaudhari, and Curtis P. Langlotz. ViLLA: Fine-Grained Vision-Language Representation Learning from Real-World Data. In *IEEE/CVF International Conference on Computer Vision (ICCV)*, 2023. URL https://doi.org/10.1109/ICCV51070.2023.02031.

Yael Vinker, Ehsan Pajouheshgar, Jessica Y. Bo, Roman Christian Bachmann, Amit Haim Bermano, Daniel Cohen-Or, Amir Zamir, and Ariel Shamir. CLIPasso: Semantically-aware Object Sketching. *ACM Trans. Graph.*, 41(4):86:1–86:11, 2022. URL https://doi.org/10.1145/3528223.3530068.

VTracer. Vtracer, 2024. URL https://www.visioncortex.org/vtracer-docs.

Junyang Wang, Haiyang Xu, Haitao Jia, Xi Zhang, Ming Yan, Weizhou Shen, Ji Zhang, Fei Huang, and Jitao Sang. Mobile-agent-v2: Mobile device operation assistant with effective navigation via multi-agent collaboration. *arXiv preprint arXiv:2406.01014*, 2024.

Zhenhailong Wang, Haiyang Xu, Junyang Wang, Xi Zhang, Ming Yan, Ji Zhang, Fei Huang, and Heng Ji. Mobile-agent-e: Self-evolving mobile assistant for complex tasks. *arXiv preprint arXiv:2501.11733*, 2025.

Zhou Wang, Alan C. Bovik, Hamid R. Sheikh, and Eero P. Simoncelli. Image Quality Assessment: From Error Visibility to Structural Similarity. *IEEE Trans. Image Procetss.*, 13(4):600–612, 2004. URL https://doi.org/10.1109/TIP.2003.819861.

Chenfei Wu, Shengming Yin, Weizhen Qi, Xiaodong Wang, Zecheng Tang, and Nan Duan. Visual ChatGPT: Talking, Drawing and Editing with Visual Foundation Models. *arXiv prepring arXiv:2303.04671*, 2023. URL https://doi.org/10.48550/arXiv.2303.04671.

Jiajun Wu, Joshua B. Tenenbaum, and Pushmeet Kohli. Neural Scene De-rendering. In *2017 IEEE Conference on Computer Vision and Pattern Recognition (CVPR)*, 2017. URL https://doi.org/10.1109/CVPR.2017.744.

Penghao Wu and Saining Xie. V*: Guided Visual Search as a Core Mechanism in Multimodal LLMs. *arXiv prepring arXiv:2312.14135*, 2023. URL https://doi.org/10.48550/arXiv.2312.14135.

Tianbao Xie, Danyang Zhang, Jixuan Chen, Xiaochuan Li, Siheng Zhao, Ruisheng Cao, Toh Jing Hua, Zhoujun Cheng, Dongchan Shin, Fangyu Lei, et al. Osworld: Benchmarking multimodal agents for open-ended tasks in real computer environments. *arXiv preprint arXiv:2404.07972*, 2024.

Ximing Xing, Haitao Zhou, Chuang Wang, Jing Zhang, Dong Xu, and Qian Yu. Svgdreamer: Text guided svg generation with diffusion model. In *Proceedings of the IEEE/CVF Conference on Computer Vision and Pattern Recognition*, pp. 4546–4555, 2024.

Kexin Yi, Jiajun Wu, Chuang Gan, Antonio Torralba, Pushmeet Kohli, and Josh Tenenbaum. Neural-Symbolic VQA: Disentangling Reasoning from Vision and Language Understanding. In *Advances in Neural Information Processing Systems 31: Annual Conference on Neural Information Processing Systems 2018 (NeurIPS)*, 2018. URL https://proceedings.neurips.cc/paper/2018/hash/5e388103a391daabe3de1d76a6739ccd-Abstract.html.

Weihao Yu, Zhengyuan Yang, Linjie Li, Jianfeng Wang, Kevin Lin, Zicheng Liu, Xinchao Wang, and Lijuan Wang. MM-Vet: Evaluating Large Multimodal Models for Integrated Capabilities. *arXiv prepring arXiv:2308.02490*, 2023. URL https://doi.org/10.48550/arXiv.2308.02490.

Xiang Yue, Yuansheng Ni, Kai Zhang, Tianyu Zheng, Ruoqi Liu, Ge Zhang, Samuel Stevens, Dongfu Jiang, Weiming Ren, Yuxuan Sun, Cong Wei, Botao Yu, Ruibin Yuan, Renliang Sun, Ming Yin, Boyuan Zheng, Zhenzhu Yang, Yibo Liu, Wenhao Huang, Huan Sun, Yu Su, and Wenhu Chen. MMMU: A Massive Multi-discipline Multimodal Understanding and Reasoning Benchmark for Expert AGI. *arXiv prepring arXiv:2311.16502*, 2023. URL https://doi.org/10.48550/arXiv.2311.16502.

Sharon Zhang, Jiaju Ma, Jiajun Wu, Daniel Ritchie, and Maneesh Agrawala. Editing Motion Graphics Video via Motion Vectorization and Transformation. *ACM Trans. Graph.*, 42(6):229:1–229:13, 2023. URL https://doi.org/10.1145/3618316.

Boyuan Zheng, Boyu Gou, Jihyung Kil, Huan Sun, and Yu Su. Gpt-4v(ision) is a generalist web agent, if grounded. In *Forty-first International Conference on Machine Learning*, 2024. URL https://openreview.net/forum?id=piecKJ2DlB.

Mingyang Zhou, Yi Ren Fung, Long Chen, Christopher Thomas, Heng Ji, and Shih-Fu Chang. Enhanced Chart Understanding via Visual Language Pre-training on Plot Table Pairs. In *Findings of the Association for Computational Linguistics: ACL 2023*, 2023a. URL https://doi.org/10.18653/v1/2023.findings-acl.85.

Shuyan Zhou, Frank F Xu, Hao Zhu, Xuhui Zhou, Robert Lo, Abishek Sridhar, Xianyi Cheng, Yonatan Bisk, Daniel Fried, Uri Alon, et al. Webarena: A realistic web environment for building autonomous agents. *arXiv preprint arXiv:2307.13854*, 2023b.

Bocheng Zou, Mu Cai, Jianrui Zhang, and Yong Jae Lee. Vgbench: Evaluating large language models on vector graphics understanding and generation. *arXiv preprint arXiv:2407.10972*, 2024.

Appendix

The appendix is organized as follows: In Appendix A, we present preliminary experiments comparing SVG and image-based representations. In Appendix B, we include details on error analyses, and in Appendix C, we describe Primal Visual Description details. Appendices D–F present additional experiments on Vtracer visual encoding quality, PVD model variants, and open-source LMM reasoner variants. Appendix G provides additional qualitative examples of PVD parsing novel concepts via composition. Appendix H presents further efforts in refining prompts for integrating PVD into LMMs. Appendix I shows the full input and output from GPT-4 for the maze-solving example depicted in Figure 2. Task prompts and newly constructed downstream task datasets can be found in Appendices J and K, respectively. In Appendix L, we include detailed statistics for all of the datasets we used.

A Preliminary Experiments on SVG Representations

We introduce a suite of probing tasks to evaluate current LMMs' capabilities in performing tasks with vector graphics. The results show that even state-of-the-art LMMs, such as GPT-4V, struggle with tasks that require precise perception of low-level primitives, such as comparing the lengths of two lines. We then investigate where this deficiency originates and propose an alternative representation, Scalable Vector Graphics (SVG), for representing such precise low-level features. We find that, compared to image-based representations, SVG representations can be more efficient for visual reasoning on vector graphics. However, they are not without their own limitations, which we will elaborate on in § A.3.

A.1 Image and SVG Representations

In the probing tasks, we include both discriminative and generative tasks, each with varying levels of emphasis on low-level visual details. Illustrations of the input and output examples are available in Figure 8. We additionally include a non-vector-graphics task, Clevr QA, which consists of realistic 3D rendered scenes. This is to test the limits of SVG representations in encoding 3D objects within realistic images. Detailed statistics of these tasks can be found in Table 13.

For each task, we consider two evaluation settings: zero-shot and fine-tuning. We explore two types of representations for the input image: (1) direct use of the image pixels, encoding them into patch embeddings with an image encoder, e.g., CLIP (Radford et al., 2021); (2) conversion of the image into SVG code using a rule-based raster-to-SVG converter (VTracer, 2024).

For fine-tuning with the image input, we instruction-finetune Llava-v1.5-7b (including the LLM-backbone and the projection layer) using Lora (Hu et al., 2022) on the training set for one epoch. For fine-tuning with the SVG input, we only fine-tune the LLM backbone of Llava-v1.5, Vicuna (Chiang et al., 2023), using Lora for one epoch, with the input image's SVG code concatenated in the context. The results are shown in Table 3. Key observations include:

(1) The SOTA open-source LMM, Llava-v1.5, struggles to achieve non-trivial performance on most probing tasks even with dedicated fine-tuning. On tasks with binary choices, Llava tends to predict homogeneous answers, disregarding differences in the input image.

(2) The SOTA closed-source LMM, GPT-4V, excels on task Line or Angle, which focuses on querying the high-level semantics of the primitive concept ("what's in the image"). However, its performance significantly decreases on tasks requiring more precise low-level perception, e.g., Angle Classification and Length Comparison.

(3) Fine-tuning the LLM backbone, Vicuna, with SVG inputs consistently outperforms fine-tuning the entire Llava model with image inputs. This highlights the potential of using SVG as an alternative representation in vector graphics.

(4) We note that SVG may inherently be inefficient in representing rendered 3D scenes and realistic images due to factors like camera perspectives, lighting, and shadows. While our focus in this work is on vector graphics, we leave the extension to other domains for future exploration.

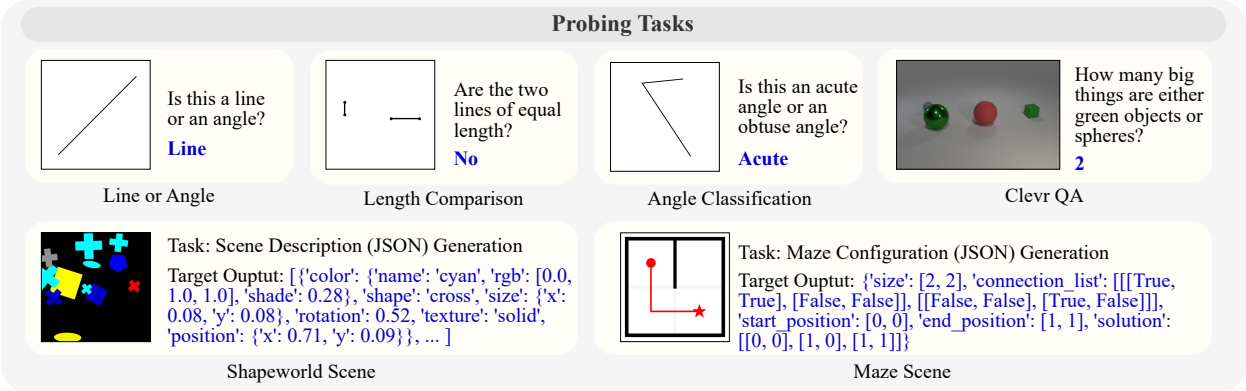

Figure 8: Illustration of the probing tasks. The four tasks at the top are question-answering tasks, while the two tasks at the bottom are scene-generation tasks. The goal of the scene-generation tasks is to generate the entire structured scene description following a predefined schema.

		Input Type	Line or Angle	Angle Classification	Length Comparison	Clevr QA
Zero-Shot	GPT-4V	Image	1.00	0.58	0.64	0.57
	GPT-4	SVG	0.45	0.47	0.60	0.36
Finetuned	Llava-v1.5-7b	Image	0.50	0.50	0.50	0.45
	Vicuna	SVG	0.93	0.70	0.99	0.54

		Input Type	Shapeworld Scene		Maze Scene		
			shape (acc↑)	position (l2↓)	connectivity (acc↑)	start-pos (acc↑)	end-pos (acc↑)
Zero-Shot	GPT-4V	Image	0.33	0.27	0.27	0.21	0.22
Finetuned	Llava-v1.5-7b	Image	0.04	0.67	0.26	0.03	0.03
	Vicuna	SVG	0.15	0.07	0.54	0.08	0.09

Table 3: Probing task results. We report the accuracy for the four question-answering tasks at the top. At the bottom, we use different metrics for different fields in the predicted scene description JSON. "acc" refers to accuracy (larger is better) while "l2" refers to the Euclidean distance between the predicted and ground truth [x, y] coordinates (lower is better). Scores with a blue background denote the better fine-tuned method compared to the SVG and Image representation. Scores with a red background denote tasks where fine-tuned methods cannot outperform zero-shot GPT-4V. Detailed analysis can be found in § A.1.

A.2 Llava's Failure Mode in Visual Reasoning with Vector Graphics

We further investigate whether the difficulty in understanding low-level visual features of Llava models stems from (1) the visual backbone itself, i.e., CLIP, or (2) the bridge between the visual backbone and the LLM backbone. We include a set of **Linear Probing** experiments on three binary classification probing tasks, where we train a simple linear classifier based on the visual backbone features (before and after projection) of the Llava model. As shown in Figure 9:

(1) In tasks requiring more precise low-level perception, such as Angle Classification and Length Comparison, CLIP embeddings are inherently less effective at capturing relevant features. Furthermore, as shown in Figure 10, in some tasks, e.g., Length Comparison, linear regression even fails to achieve 90%+ training accuracy after 10 epochs of training, struggling to converge.

(2) When connected to an LLM using the projection layer, the visual features in Llava become less effective for low-level visual reasoning. Additionally, there is a significant gap between linear probing and instruction fine-tuning performance. These results suggest that even if the backbone does preserve useful features, the LLM cannot effectively leverage those visual tokens after projection.

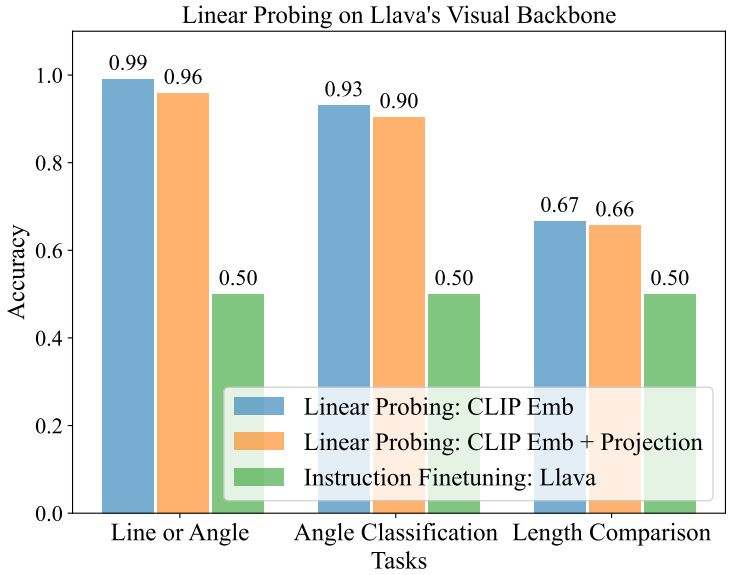

Figure 9: The average accuracy of linear probing, computed across ten epochs. Detailed training and testing scores for each epoch can be found in Figure 10. The results demonstrate that (1) CLIP embeddings are less effective for tasks requiring precise perception, such as Length Comparison, in comparison to tasks that emphasize on higher-level semantics, such as Line or Angle; (2) connecting to an LLM through the widely-used Llava-style architecture results in further diminished performance on tasks involving low-level visual details.

We hypothesize that the failure mode likely stems from the multimodal pretraining and instruction-tuning paradigm, where the tasks are biased towards high-level semantics, such as image captioning (Lin et al., 2014; Sidorov et al., 2020) and natural-image-based VQA (Goyal et al., 2017; Krishna et al., 2017; Marino et al., 2019; Schwenk et al., 2022). The training mixtures (Liu et al., 2023b;a; Dai et al., 2023; Chen et al., 2023a) for current LMMs predominantly focus on high-level features of images, providing little incentive for models to retain low-level visual details. For example, the caption of an image containing a 2D maze, such as the one shown in Figure 2, is likely to be "A 2×2 maze with black lines, a red circle and a star." and may not include detailed configurations of the mazes, such as the precise locations of the walls, the red circle, and the red star.

A.3 Remaining Challenges of Using SVG Representations

Although we have demonstrated that SVG can serve as a promising alternative representation for reasoning about vector graphics, we identify several remaining challenges:

(1) Pretrained LLMs, including the most capable ones such as GPT-4 (OpenAI, 2023a), possess limited out-of-the-box understanding of SVG code. This limitation is evidenced by the low zero-shot performance of GPT-4 with SVG input (see row 2 in Table 3).

(2) Even after finetuning, the SVG-based LLM may still underperform zero-shot GPT-4V on certain tasks, particularly those involving complex scenes, such as Shapeworld Scene and Maze Scene. In these instances, the SVG code becomes excessively verbose. These findings suggest that learning a model to directly comprehend the raw SVG code of an entire image poses significant challenges.

(3) A fundamental challenge, irrespective of the chosen representation for visual input, is the lack of generalization capability to unseen tasks and various vector graphics image domains. If we rely on existing LMM training mixtures, even any image can be converted into SVG code, the tasks remain biased towards high-level semantics. In addition, it is infeasible to directly manually construct and annotate ⟨SVG, question, answer⟩ pairs covering diverse tasks with vector graphics.

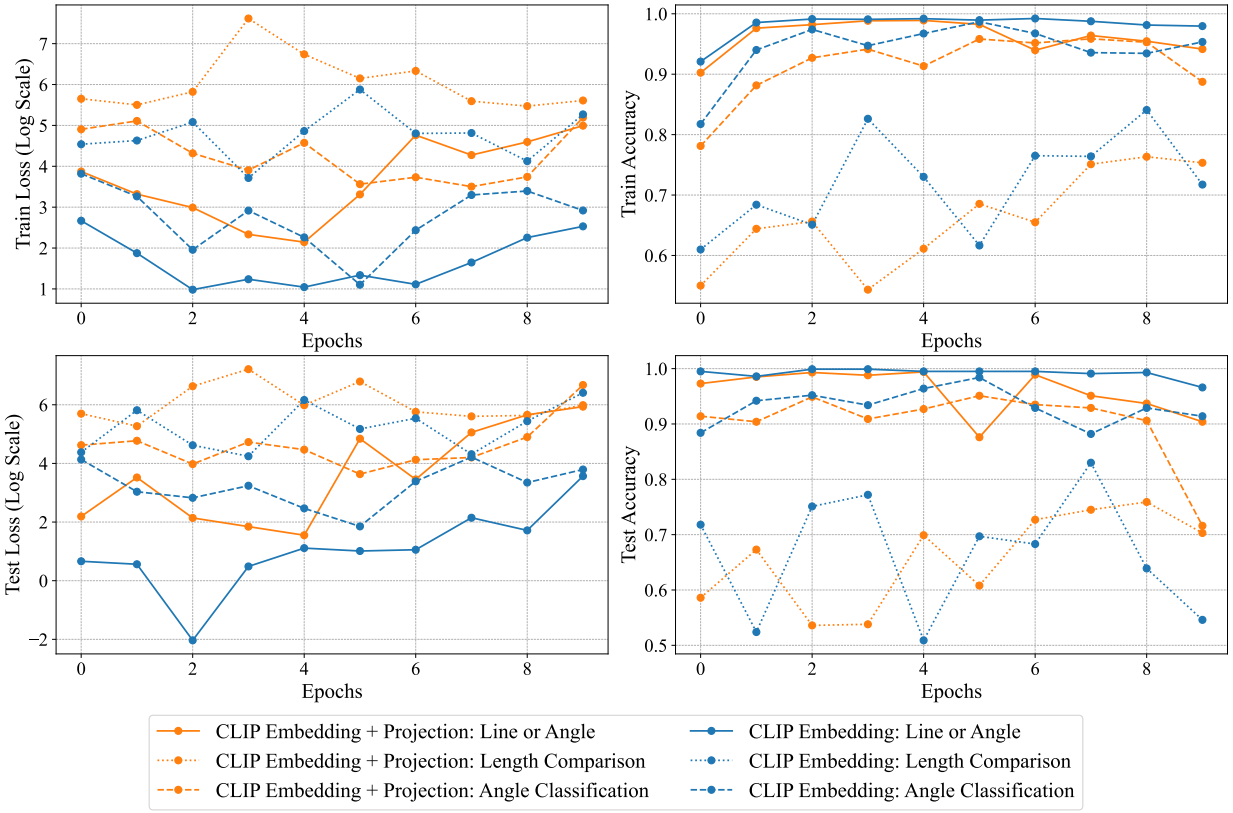

Figure 10: Linear probing training details: Different line styles represent different tasks, while different colors refer to different visual embeddings used for training the linear classifier. The training loss (top-left) shows that the projected embedding (orange lines) learns at a slower pace compared to the original CLIP embedding (blue lines). The training accuracy (top-right) reveals that for certain tasks, such as Length Comparison, the model continues to struggle with overfitting the training set even after 10 epochs.

These challenges motivated us to propose another layer of abstraction, the Primal Visual Description, aimed at bridging the gap between low-level perception and high-level language reasoning on downstream tasks.

B Error Analysis Details

As introduced in § 2, the proposed VDLM consists of two stages focused on perception—namely, Image-to-SVG and SVG-to-PVD, and one stage focused on reasoning, i.e., PVD-to-final answer. We aim to investigate the errors in both the perception and reasoning modules.

For each task, we manually examine 10 error cases and determine whether the error primarily stems from the perception stage or the reasoning stage. We task a human with reviewing the reconstructed image from the PVD representation and assessing the question of the task instance. If, for a human, the reconstructed image is still insufficient for solving the task, we classify this error as a perception error. Otherwise, it is categorized as a reasoning error. Figure 11 illustrates the distribution of errors between perception and reasoning stages. We further identify some typical categories of perception and reasoning errors as follows:

Common perception errors. (1) **Novel shapes not covered by the Primal Visual Description (PVD)**: For example, as visualized in Figure 12, the Shapeworld dataset includes a "semicircle" shape type which is not in the PVD ontology; we see that the learned SVG-to-PVD model tends to predict it as an ellipse. This perception error directly contributes to the inferior performance of VDLM-mm compared to GPT-4o on the Shapeworld tasks, as shown in Table 1.

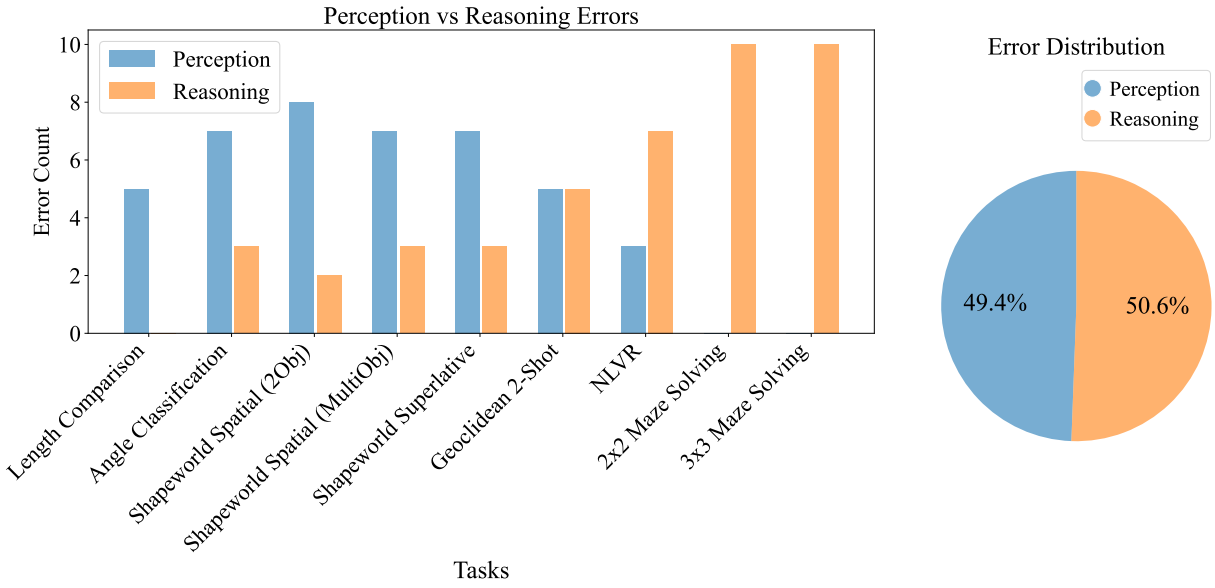

Figure 11: Error distribution by VDLM-txt between perception and reasoning on low-level vector graphics reasoning.

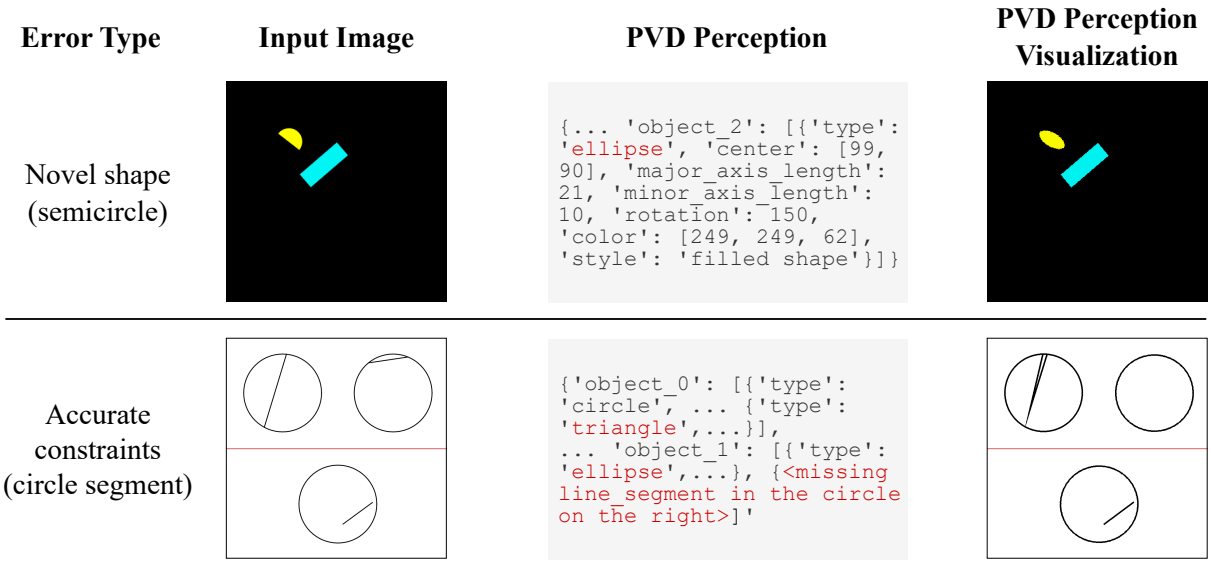

Figure 12: Perception error examples. The example at the top illustrates an error wherein the SVG-to-PVD model predicts a semicircle as an ellipse. The example at the bottom demonstrates that the SVG-to-PVD model struggles to decode overlapping primitives with accurate constraints, such as a segment of a circle.

(2) **Accurate constraints between primitives**: Although the PVD accommodates scenarios where multiple objects of the same color overlap, the attributes, e.g., position, of each object are decided independently and randomly. Thus, the SVG-to-PVD model often fails to capture intentional constraints between objects; for example, a line that perfectly segments a circle. These constraints are particularly emphasized in the Geoclidean 2-shot Learning task (Figure 12), where VDLM struggles to outperform GPT-4V and GPT-4o.

(3) **Very small objects**: During inference, the iterative decomposition process heuristically ignores SVG paths that only contribute only minor differences to the reconstructed image. This method effectively reduces

Error Type	Input Image	PVD Perception Visualization	Reasoning Model (GPT-4) Response
Discovering constraints (Rhombus v.s. Quadrilateral)	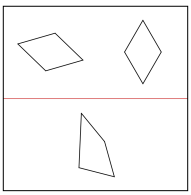	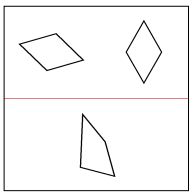	To analyze the given JSON and identify the pattern and constraints of the reference and test concepts, let's break down the information provided for each object: 1. **Object 0** (Test Example): - Type: Polygon - Vertices: [(304, 416), (395, 527), (433, 665), (295, 629)] - Characteristics: Outlined shape, black color, polygon with 4 vertices. 2. **Object 1** (Reference Example 1): - Type: Polygon ... 3. **Object 2** (Reference Example 2): - Type: Polygon ... Given the descriptions, the reference examples (Object 1 and Object 2) and the test example (Object 0) are all polygons with 4 vertices, suggesting they are quadrilaterals... Given the information and assuming the concept involves quadrilaterals without requiring them to have uniform angles or sides (since we cannot precisely measure them from the given data), the test example appears to follow the same broad concept of being a quadrilateral as the reference examples.
Algorithmic reasoning (Inferring maze connectivity)	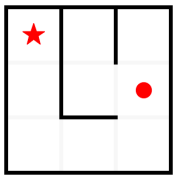	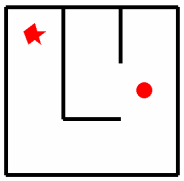	By examining the grid lines, we can determine where the walls are and thus infer the connections. However, the JSON doesn't directly specify the walls between cells, but we can deduce this from the absence of grid lines between cells. For simplicity, let's assume a fully connected grid without internal walls (as the JSON doesn't specify walls between cells explicitly), and then adjust based on typical maze patterns: - **Vertical Connections:** All true, indicating no vertical walls between cells. - **Horizontal Connections:** All true, indicating no horizontal walls between cells. ... {"solution": "[(1, 1), (0, 0)]"}

Figure 13: Reasoning error examples: The example at the top demonstrates that the reasoning model fails to uncover the deeper constraints within the perceived polygons. It is able to recognize that they are all quadrilaterals but unable to further discern that the reference concepts are rhombuses with four equal sides, while the test concept is not. The example at the bottom illustrates that the reasoning model struggles to infer connectivity based on the perceived grid, thus failing to provide the correct solution.

noise from the rule-based image-to-SVG converter but may omit very small objects in some cases. Adjusting this threshold is necessary for specific scenarios.

Common reasoning errors. (1) **Discovering intentional constraints**: Without specific queries, the reasoning model can fail to identify intentional constraints. For example, differentiating a rhombus from a general quadrilateral, as shown in Figure 13.

(2) **Handling ambiguity**: Visual inputs sometimes provide useful inductive biases that can help the model better understand the task or make reasonable assumptions when the instructions are ambiguous. For instance, when presenting an angle in an image and asking whether it is an acute or obtuse angle, as in Figure 4, it is visually straightforward to assume that the angle is defined by the middle point as the vertex with rays extending outwards. However, without such visual cues, reasoning over pure symbolic representations makes it challenging to infer which angle the question refers to among the detected undirected edges. To mitigate ambiguity, adding more precise instructions for VDLM-txt is necessary in some tasks.

(3) **Algorithmic reasoning**: Language-based reasoners can struggle with complex multi-step reasoning tasks, such as inferring the connectivity (Figure 13) of a maze using the vertices and edges of the grid in pixel coordinates, or counting the number of objects located within a certain box.

C Primal Visual Description (PVD) Details

PVD JSON schema definition: See Figure 14.

Types	Schema	Example
Circle	`{ "type": "circle", "center": [x, y], "radius": r, "color": [r, g, b], "style": "filled shape" or "outlined shape", "line_width": d (if style is "outlined") }`	`{ "type": "circle", "center": [205, 210], "radius": 117, "color": [193, 190, 165], "style": "outlined shape", "line_width": 9 }`
Ellipse	`{ "type": "ellipse", "center": [x, y], "major_axis_length": l1, "minor_axis_length": l2, "rotation": o, "color": [r, g, b], "style": "filled shape" or "outlined shape", "line_width": d (if style is "outlined") }`	`{ "type": "ellipse", "center": [278, 166], "major_axis_length": 147, "minor_axis_length": 60, "rotation": 16, "color": [85, 220, 98], "style": "filled shape" }`
Rectangle Triangle Polygon	`{ "type": "rectangle" or "triangle" or "polygon", "vertices": [[x1, y1], [x2, y2], ...] "color": [r, g, b], "style": "filled shape" or "outlined shape", "line_width": d (if style is "outlined") }`	`{ "type": "triangle", "vertices": [[452, 418], [298, 113], [266, 255]], "color": [165, 170, 141], "style": "filled shape", }`
Line Segment	`{ "type": "line_segment", "vertices": [[x1, y1], [x2, y2]] "color": [r, g, b], "line_width": d }`	`{ "type": "line_segment", "vertices": [[822, 114], [93, 20]], "color": [166, 32, 97], "line_width": 10 }`
Grid	`{ "type": "grid", "vertices": [[x1, y1], [x2, y2], ...], "edges": [[[x1, y1], [x2, y2]], ...], "color": [r, g, b], "line_width": d }`	`{ "type": "grid", "vertices": [[73, 214], [73, 640], [215, 214], [215, 640]], "edges": [[[73, 214], [73, 640]], [[215, 214], [215, 640]], [[73, 640], [215, 640]]] "color": [23, 31, 120], "line_width": 3 }`
Path	`{ "type": "path", "vertices": [[x1, y1], [x2, y2], ...], "edges": [[[x1, y1], [x2, y2]], ...], "color": [r, g, b], "line_width": d }`	`{ "type": "path", "vertices": [[59, 69], [17, 330], [61, 77]], "edges": [[[59, 69], [17, 330]], [[17, 330], [61, 77]]] "color": [98, 28, 0], "line_width": 5 }`
Graph	`{ "type": "line drawing", "vertices": [[x1, y1], [x2, y2], ...], "edges": [[[x1, y1], [x2, y2]], ...], "color": [r, g, b], "line_width": d }`	`{ "type": "line drawing", "vertices": [[399, 497], [433, 823], [483, 570], [531, 443], [534, 578]], "edges": [[[399, 497], [483, 570]], [[531, 443], [534, 578]], [[483, 570], [534, 578]], [[483, 570], [433, 823]], [[534, 578], [433, 823]]] "color": [254, 230, 139], "line_width": 9 }`

Figure 14: PVD JSON schema definition.

Generation procedures (Single Object):

- **Circle:** Randomly sample a center and a radius to draw a circle within the canvas.

	Style	Concept	# Instances
Single Object	Filled or Outlined	Circle	10K
		Ellipse	10K
		Rectangle	10K
		Triangle	10K
		Polygon	20K
		Line Segment	10K
		Grid	10K
		Path	10K
		Graph	10K
Composition	Filled	Circle	5K
		Rectangle	5K
		Triangle	5K
		Line Segment	5K
	Outlined	Circle	10K
		Rectangle	10K
		Triangle	10K
		Line Segment	10K
		Total	160K

Table 4: PVD 160K dataset statistics.

- **Ellipse:** Randomly sample a center, a major axis, and a minor axis, then randomly rotate by an angle. Verify if the ellipse is largely within the canvas; if not, try again.
- **Rectangle:** Randomly sample a top-left corner, a width, and a height, then randomly rotate by an angle. Verify if the rectangle is largely within the canvas; if not, try again.
- **Triangle:** Randomly sample three points as vertices to draw a triangle. Check if the area is larger than a threshold; if not, try again.
- **Polygon:** Randomly sample $N \in [5, 20]$ points. Order the points with respect to the centroid so that no intersections will happen when connected with a polyline. Draw a polygon with the sampled points. Check if the polygon has an area larger than a threshold; if not, try again.
- **Path:** Randomly and iteratively sample $N \in [3, 16]$ points, connect the newly sampled point with the previous point to form a line segment. Verify if the newly added line segment does not intersect with any of the previous line segments; if yes, resample the point.
- **Grid:** Sample a grid of points with a size $M \times N$ where $M, N \in [2, 6]$. First, use Depth First Search (DFS) algorithm to connect all grid vertices into a connected graph. Then randomly add additional edges between adjacent vertices.
- **Graph:** Randomly sample $N \in [4, 16]$ points. First, use Kruskal's algorithm (Kruskal, 1956) to find a Minimum Spanning Tree that connects all the points. Then randomly add additional edges to the graph.

Generation procedures (Composition): Iteratively draw shapes on the canvas chosen from the following set of object types: ["circle", "rectangle", "triangle", "line segment"]. After the first shape is drawn, at each iteration, the later shapes are constrained to have the same color as the previous shapes. We ensure overlap between the newly added shape and the previous shapes, while making sure that the intersection ratio does not exceed a predefined threshold. This prevents cases where one shape entirely contains another, making it impossible to decode into individual Primal Visual Description elements.

PVD 160K dataset: Using the aforementioned generation procedure, we generate a large-scale dataset containing 160K ⟨SVG, PVD⟩ pairs for training the LLM-based SVG-to-PVD model. The detailed configuration can be found in Table 4.

	SSIM	DINOv2 Score	CLIP Score
w/o aug	0.892	0.874	0.886
w/ aug	**0.895**	**0.893**	**0.893**

Table 5: Impact of the data augmentation (Gaussian Blur and Pixel Noise detailed in §2.2) on SVG-to-PVD model perception performance.

Data augmentation details: To enhance the robustness of the SVG-to-PVD model to images with various sizes and quality, we introduce the following randomized data augmentation during data generation.

- **Random pixel noise**: Probability (how often to apply the augmentation): 0.1; Ratio range (what portion of the selected area will be filled with noise pixels): (0.01, 0.05); Intensity range (the intensity of the noise pixels): (0.1, 1.0); Dilate range (how many pixels will the selection area be extended from the boundary): (1, 3) in pixels; Noise size: (1, 3) in pixels.
- **Gaussian blur**: Probability (how often to apply the augmentation): 0.1; Radius: (0.1, 0.5).

Table 5 shows the ablation study with and without the data augmentations.

D Image-to-SVG Visual Encoding Quality

VTracer Encoding Quality. As introduced in Section 2.1, the first step of our proposed perception module is to encode a raster image into an SVG representation using VTracer, a rule-based converter that we found yields near-perfect reconstructions for vector-graphic–style inputs. To verify this, we convert the VTracer-encoded SVGs back into PNG images and compare them with the originals. The results are presented in Table 6.

Task	SSIM	DINOv2 Score	CLIP Score
Angle Classification	0.990	0.991	0.997
Length Comparison	0.994	0.970	0.986
Shapeworld Spatial 2Obj	0.997	0.984	0.995
Shapeworld Spatial mObj	0.991	0.984	0.988
Shapeworld Superlative	0.991	0.982	0.987
NLVR	0.994	0.989	0.993
Geoclidean	0.648	0.994	0.995
Maze 2×2	0.998	0.906	0.775
Maze 3×3	0.998	0.998	0.989
ALL	0.956	0.978	0.967

Table 6: VTracer SVG encoding reconstruction metrics. The exceptionally low SSIM score on Geoclidean is due to the fact that most pixels are transparent. Since we compute SSIM only on non-transparent regions, the score becomes more sensitive to slight pixel differences. However, the reconstruction appears visually near-perfect across all tasks, as reflected by the high DINOv2 score.

We observe near-perfect reconstruction quality from VTracer. For reference, the average reconstruction quality from the PVD representation (after SVG-to-PVD conversion) is SSIM = 0.895, DINOv2 Score = 0.880, and CLIP Score = 0.893, indicating that most perception errors arise during the SVG-to-PVD step. However, as discussed in Section 2.2, although SVG preserves all low-level features, it is extremely verbose and noisy—making it unintelligible to LLMs and LMMs. This observation motivates the development of the intermediate PVD representation.

Impact of VTracer Error to the End-task Performance. To further investigate whether imperfections in SVG encoding significantly affect end-task performance. We sort the instances for each task with respect to VTracer reconstruction quality, using the aggregated metric: SSIM + DINOv2 score + CLIP score. The

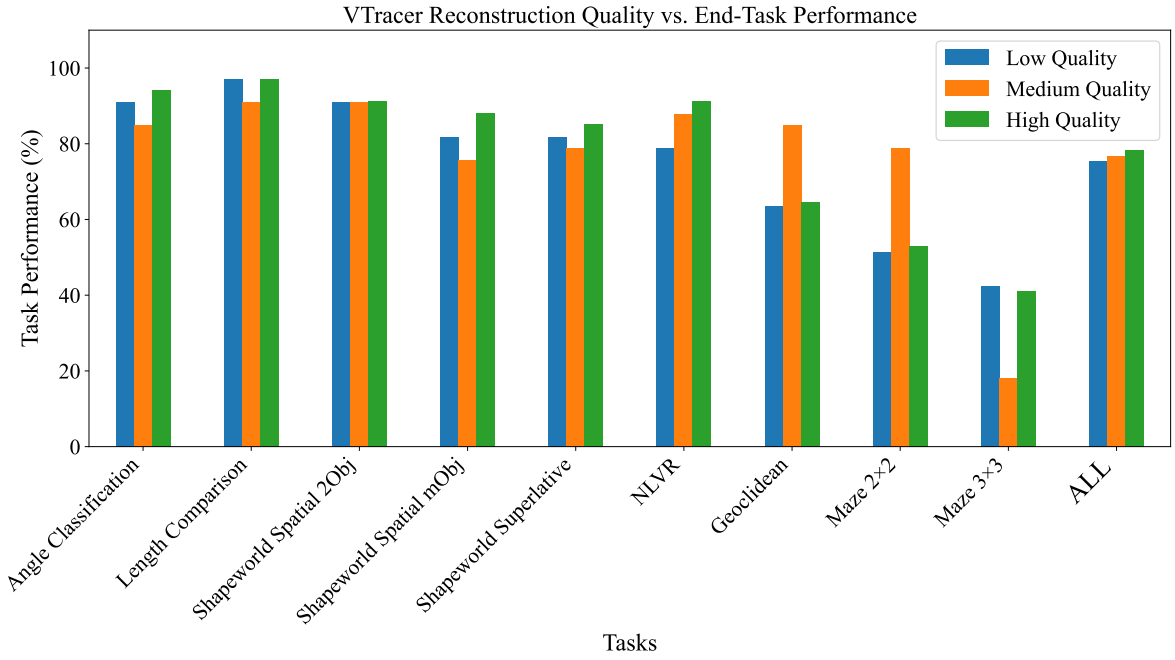

Figure 15: Impact of SVG encoding quality on end-task performance.

instances are then grouped into three bins corresponding to low, medium, and high VTracer quality. We examine the end-task performance (VDLM-mm + GPT-4o) of these groups to investigate whether performance is sensitive to VTracer errors. In Figure 15, we show the average accuracy on each task for each bin. Note that each bin has about 33 instances.

Overall, we observe that end-task performance is fairly robust to vectorization errors, while also exhibiting a trend similar to what we reported in Section 4.1, i.e., a positive correlation between perception quality and end-task performance.

E Additional Ablations on PVD Perception

PVD Model	SSIM ↑	DINOv2 Score ↑	CLIP Score ↑
SVG-to-PVD (Mistral-7B)	0.895	0.880	0.893
SVG-to-PVD (Qwen2.5-7B)	0.889	0.876	0.880

Table 7: Perception metrics of different SVG-to-PVD models.

Reasoner	PVD Model	AC	LC	SW-S 2Obj	SW-S mObj	SW Sup	NLVR	Geo	Maze 2×2	Maze 3×3	All
GPT-4o	–	0.63	0.57	0.97	0.82	0.92	0.81	0.71	0.46	0.08	0.663
GPT-4o	Mistral-7B	0.90	0.95	0.91	0.82	0.82	0.86	0.71	0.61	0.34	0.769
GPT-4o	Qwen2.5-7B	0.82	0.98	0.99	0.79	0.89	0.83	0.68	0.70	0.29	0.774

Table 8: End-task performance with different SVG-to-PVD models.

Different LLM choices for SVG-to-PVD model. We investigate the effect of using a different LLM for SVG-to-PVD translation. Specifically, we train a Qwen-2.5-7B[¶] base model on the PVD-160k dataset using the same number of epochs as our original model. We observe comparable perception and end-task performance to our original PVD model, which is based on Mistral-7B. Table 7 and Table 8 report the perception scores and end-task performance of SVG-to-PVD models trained with different LLM backbones. These results suggest that the SVG-to-PVD translation process is robust to the choice of LLM.

[¶] https://huggingface.co/Qwen/Qwen2.5-7B

PVD Model	Training Epochs	Final Loss ↓
SVG-to-PVD (Qwen2.5-7B)	3 epochs	0.052
SVG-to-PVD (Mistral-7B)	3 epochs	0.051
PNG-to-PVD (Qwen2.5-VL-7B)	3 epochs	0.243

Table 9: Comparison of training loss between the PNG-to-PVD and SVG-to-PVD models.

PVD Model	SSIM ↑	DINOv2 Score ↑	CLIP Score ↑
SVG-to-PVD (Mistral-7B)	0.895	0.880	0.893
SVG-to-PVD (Qwen2.5-7B)	0.889	0.876	0.880
PNG-to-PVD (Qwen2.5-VL-7B)	0.262	0.320	0.385

Table 10: Comparison of perception metrics between the PNG-to-PVD and SVG-to-PVD models.

Ablation with PNG-to-PVD model. To further validate the design choice of using SVG for initial visual encoding, we compare it with directly training a PNG-to-PVD model using a large multimodal model. Specifically, we train Qwen2.5-VL-7B [‖] on the same PVD-160k dataset, where the inputs are png images and the target outputs are PVD strings. Table 9 and Table 10 show the comparison between the PNG-to-PVD and SVG-to-PVD models in terms of final training loss and perception metrics. Using identical hyperparameters, we find that directly translating PNG to PVD is significantly less effective, as evidenced by a much higher loss and substantially lower perception performance. We observe that the PNG-to-PVD model rarely produces valid PVD JSON outputs and yields significantly worse reconstruction performance (entirely not usable for downstream reasoning).

F Additional Experiments Using Open-Source LMMs as Reasoners

Reasoner	PVD Model	AC	LC	SW-S 2Obj	SW-S mObj	SW Sup	NLVR	Geo	Maze 2×2	Maze 3×3	All
Qwen2.5-VL-72B	–	0.78	0.75	0.98	0.75	0.92	0.72	0.67	0.64	0.15	0.707
Qwen2.5-VL-72B	Mistral-7B	0.59	0.96	0.96	0.78	0.89	0.69	0.73	0.66	0.28	0.727

Table 11: End-task performance with open-source LMM reasoners.

We added new experimental results demonstrating that VDLM can also work effectively with recent open-source LMMs. Specifically, we use Qwen-2.5-VL-72B[**] as the reasoner to compare performance with and without the inclusion of PVD representations. Across 9 tasks, we observe a 2% overall improvement.

G Additional Qualitative Examples on PVD Parsing Novel Concepts

We highlight that our PVD ontology constitutes a minimal but powerful set of primitives for expressing shapes in vector graphics. We demonstrate that the current PVD model shows promise in approximating novel shapes through composition. In Figure 16, we show several examples of the PVD model parsing novel concepts such as "star," "cross," and "circle segment."

H Further Exploration in Prompt Engineering

Observing that the PVD representation can sometimes be inaccurate and may degrade performance (i.e., on ShapeWorld tasks), we explore introducing a verification step in the prompt. Specifically, we instruct the model to first "double-check whether the objects in the PVD perception match the objects in the image." We find that this step can enhance performance on tasks where the initial image-only baseline is already reasonably strong. Table 12 shows the performance comparison on ShapeWorld tasks with the same LMM reasoner and PVD representation.

[‖] https://huggingface.co/Qwen/Qwen2.5-VL-7B-Instruct
[**] https://huggingface.co/Qwen/Qwen2.5-VL-72B-Instruct

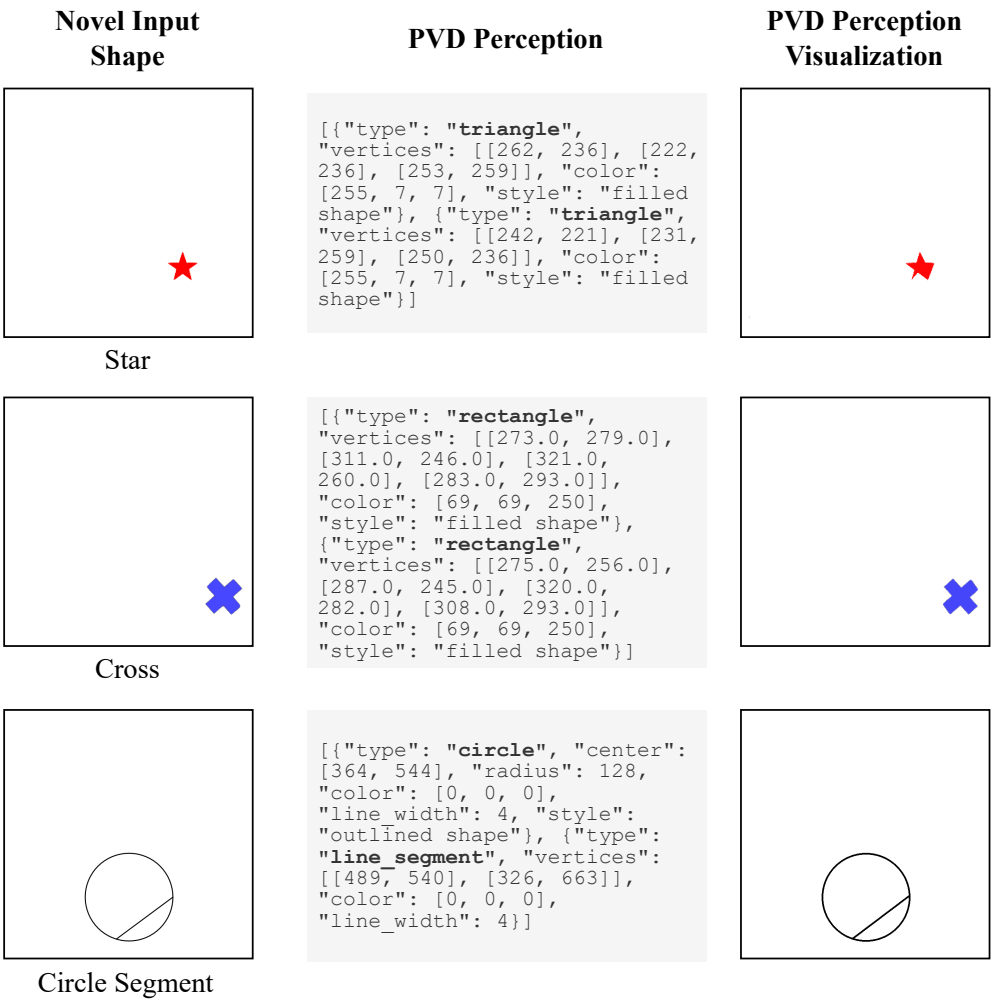

Figure 16: Qualitative examples on PVD model approximating novel concepts.

Prompt Version	Reasoner	PVD Model	SW-S 2Obj	SW-S mObj	SW Sup
-	GPT-4o	-	0.97	0.81	0.92
Original	GPT-4o	Mistral-7B	0.91	0.82	0.82
New	GPT-4o	Mistral-7B	0.98	0.81	0.88

Table 12: ShapeWorld task performance with new prompt.

I Full Response of the Example in Figure 2

See Figure 17 for the full input prompt and the generated response from GPT-4 on the 2×2 maze-solving task shown in Figure 2.

J Task Prompts

Figure 18 shows the prompts for models with only image representations as visual inputs.

Figures 19-27 show the prompts for VDLM, where {perception} will be filled with the aggregated Primal Visual Description perception result, and the orange text are instance-specific inputs such as the question. For VDLM-mm, the original image input will be preserved and feed to the LMM reasoner along with the

filled prompt. Since the reasoning in VDLM-txt is based solely on the PVD representation which is purely textual, task instructions that assume visual inputs can become ambiguous. For example, in the task Angle Classification, it is unclear which angle the question is referring to if we are only given the coordinates of two undirected edges. Therefore, we design task-specific prompts that remove such ambiguity. Another noteworthy point is that, in contrast to visual inputs that naturally accommodate a degree of imprecision, symbolic representations lack such inherent leniency. For instance, even if two line segments differ by only one pixel in length, they might be considered identical in visual representations, but symbolic representations would likely identify them as different. To reintroduce a level of tolerance in tasks that involve arithmetic reasoning, such as length comparison, we incorporate task-specific instructions to account for a reasonable margin of error, like 5%.

K Newly Constructed Downstream Task Datasets

Angle Classification. We use the Geoclidean data generator[††] to generate images containing a single acute or obtuse angle with randomized orientations and ray lengths. The domain-specific language for generating the two concepts are shown as follows:

- Acute Angle:

```
"l1* = line(p1(), p2())",
"c1* = circle(p1(), p2())",
"c2* = circle(p2(), p1())",
"l2* = line(p3(c1, c2), p4(c1, c2))",
"l4 = line(p5(l1, l2), p7(l1))",
"l5 = line(p6(l2), p7(l1))"
```

- Obtuse Angle:

```
"l1* = line(p1(), p2())",
"c1* = circle(p1(), p2())",
"c2* = circle(p2(), p1())",
"l2* = line(p3(c1, c2), p4(c1, c2))",
"l3* = line(p5(l1, l2), p6(l2))",
"l4* = line(p5(l1, l2), p7(l1))",
"l5* = line(p6(l2), p7(l1))",
"l6* = line(p8(l3, l4), p9(l5))",
"l100* = line(p5(c1, c2), p10(l6))",
"c101* = circle(p5(c1, c2), p10(l6))",
"c102* = circle(p10(l6), p5(c1, c2))",
"l101* = line(p100(c101, c102),
p101(c101, c102))",
"l7 = line(p11(l100, l101), p6(l2))",
"l8 = line(p11(l100, 101), p7(l1))"
```

Length Comparison. We use matplotlib[‡‡] to plot two non-intersecting line segments on a canvas. These line segments may either be of identical length or of differing lengths. In scenarios where the lengths vary, we ensure the discrepancy is substantial (exceeding 15% relative to the length of the shorter line segment) to ensure perceptibility. The orientation of each line segment is determined independently and randomly, being either horizontal or vertical.

[††] https://github.com/joyhsu0504/geoclidean_framework
[‡‡] https://matplotlib.org/stable/

Maze Solving. We leverage the maze-dataset package[§§] to generate 2D unsolved mazes along with their corresponding ground truth solutions. We use "circle" shape to denote the start position and "star" shape to denote the end position. We generate two subsets featuring 2×2 and 3×3 maze configurations.

L Dataset Statistics

		# Training Instances	# Eval Instances
Probing Tasks	Line or Angle	10K	1K
	Angle Classification	10K	1000
	Length Comparison	10K	1000
	Clevr QA	36K	1000
	Shapeworld Scene	15K	100
	Maze Scene	10K	600
Zero-Shot Downstream Tasks	Angle Classification	-	100
	Length Comparison	-	100
	Shapeworld Spatial Reasoning (2Obj)	-	100
	Shapeworld Spatial Reasoning (MultiObj)	-	100
	Shapeworld Superlative	-	100
	NLVR	-	100
	Geoclidean 2-shot Learning	-	100
	2×2 Maze Solving	-	100
	3×3 Maze Solving	-	100
	VGBench-QA Category	-	100
	VGBench-QA Color	-	100
	VGBench-QA Usage	-	100

Table 13: Statistics of the probing tasks (§ A.1) and the downstream tasks (§ 3). The GPT-4(V) zero-shot results on probing tasks are reported on 100 randomly sub-sampled instances from the entire eval split.

Detailed statistics of the probing tasks used in § A and the zero-shot downstream tasks mentioned in § 3 can be found in Table 13.

[§§] https://github.com/understanding-search/maze-dataset/tree/main

Input Prompt

The following JSON contains an approximated perception of a 2x2 maze. Each object (potentially including the background) is represented by a list of geometric shapes. If the object contains multiple shapes, it is a composite object. The (x, y) coordinates for the vertices and edges correspond to the width and height position in pixels, and (0, 0) is the top-left corner of the image.

--- perception ---
{'object_0': [{'type': 'rectangle', 'vertices': [[0.0, 336.0], [0.0, 0.0], [336.0, 0.0], [336.0, 336.0]], 'color': [253, 253, 253], 'style': 'filled shape'}], 'object_1': [{'type': 'grid', 'vertices': [[16, 16], [16, 164], [16, 312], [172, 16], [172, 164], [172, 312], [328, 16], [328, 164], [328, 312]], 'edges': [[[16, 16], [16, 164]], [[16, 16], [172, 16]], [[16, 164], [16, 312]], [[16, 164], [172, 164]], [[172, 16], [328, 16]], [[16, 312], [172, 312]], [[328, 16], [328, 164]], [[172, 312], [328, 312]], [[328, 164], [328, 312]]], 'color': [0, 0, 0], 'line_width': 10}], 'object_2': [{'type': 'circle', 'center': [94, 94], 'radius': 14, 'color': [255, 4, 4], 'style': 'filled shape'}], 'object_3': [{'type': 'triangle', 'vertices': [[262, 236], [222, 236], [253, 259]], 'color': [255, 7, 7], 'style': 'filled shape'}, {'type': 'triangle', 'vertices': [[242, 221], [231, 259], [250, 236]], 'color': [255, 7, 7], 'style': 'filled shape'}]}

In the 2x2 maze, walls are depicted by a grid of black lines between cells and along the perimeter. The maze cells are defined within the grid. The start position is marked by a red circle, and the end position by a red star. The position of each cell can be represented by coordinates (row, column), beginning from the top-left corner as (0, 0). Here, 'row' corresponds to the vertical dimension (height) of the image, and 'column' to the horizontal dimension (width).

Perform the following steps to solve the maze:
(1) Infer the connectivity of the cells using a connection list. For example, a 2x2 maze should have a `connection_list` containing two sublisits with dimension 1x2 and 2x1. For i in range(0, 1) and j in range(0, 2), `connection_list[0][i][j]` is `True` if cell `(i, j)` is vertically connected to cell `(i+1, j)` without being seperated by a wall. Similarly, for j in range(0, 1) and i in range(0, 2), `connection_list[1][i][j]` is `True` if cell `(i, j)` is horizontally connected to cell `(i, j+1)` without being seperated by a wall.
(2) Infer the start position and end position of the maze in the row-column format.
(3) Solve the maze by finding a path from the start position to the end position.
You MUST provide your final answer, and the answer should follow this format: {"solution": "a list of (row, column) coordinates"}.

GPT-4 Response

To solve the maze based on the provided JSON data, let's break down the steps as required:

Step 1: Infer the Connectivity of the Cells

Given the grid lines and their coordinates, we can infer the connectivity between cells. **The grid lines form the boundaries of a 2x2 maze, meaning there are 3 vertical lines and 3 horizontal lines that define the cells. By examining the edges in the JSON, we can determine where the walls are and thus infer which cells are connected.**

- Vertical connections (`connection_list[0]`): There are no vertical walls inside the maze, so both cells in the first column are connected to their respective cells in the second column.
- Horizontal connections (`connection_list[1]`): There is a horizontal wall between the two cells in the first row, meaning there's no direct connection between them. However, the cells in the second row are connected.

Therefore, the `connection_list` can be represented as:
- Vertical connections: `[[True, True]]`
- Horizontal connections: `[[False], [True]]`

Step 2: Infer the Start and End Positions

- The **start position** is marked by a **red circle**, which is located at approximately `[94, 94]`. This places it in the **top-left cell, or `(0, 0)`**.
- The **end position** is marked by **a composite red shape resembling a star, located in the bottom-right cell**, which can be inferred from the coordinates of the triangles forming the star shape. This **places the end position at `(1, 1)`**.

Step 3: Solve the Maze

Given the connectivity and the start/end positions, we can find a path from the start to the end. The path, considering the connectivity and the positions, would be:
1. Start at `(0, 0)`.
2. Move right to `(0, 1)`.
3. Move down to `(1, 1)`.

Thus, the solution path is: `[(0, 0), (0, 1), (1, 1)]`.

Final Answer

```json
**{"solution": "[(0, 0), (0, 1), (1, 1)]"}**
```

Figure 17: Full input prompt and GPT-4 response of the 2x2 maze solving example in Figure 2. The blue part in the input prompt indicates the generated Primal Visual Description (PVD) of the entire image.

Is this an acute angle or an obtuse angle? Answer with "Acute" or "Obtuse".

Acute-or-Obtuse

Are these two lines of equal length? Choose "Yes" or "No".

Length-Comparison

Given a 2d scene containing objects with the following attributes:
--- Attribute Ontology ---
- color: ['red', 'green', 'blue', 'yellow', 'magenta', 'cyan', 'gray']
- shape: ['square', 'rectangle', 'triangle', 'pentagon', 'cross', 'circle', 'semicircle', 'ellipse']

Think step by step and answer the following question:
{question}

You MUST provide your final answer, and the answer should follow this format: {{"answer": "yes" or "no"}}

Shapeworld

Given an image containing three boxes with light grey background, horizontally layed out. The boxes are seperated by two dark grey rectangles placed vertically, which are referred to as walls. An "edge" is referred to as the boundary of the image. A "base edge" is referred to as the bottom boundary. If an object's boundary is located very close to an edge or a wall (e.g., within 10 pixels), it is considered as "touching". Each box contains a set of shapes. There are two types of images: "Tower", and "Scatter". In "Tower" images, each box contains only squares stacked in towers with up to 4 squares. In "Scatter" images, each box contains scattered objects of different sizes and shapes.

Think step by step to answer the following question:
{question}

You MUST provide your final answer, and the answer should follow this format: {{"answer": "yes" or "no"}}

NLVR

The top part of the scene provides {n_shot} reference examples of a Euclidean geometry concept. A Euclidean geometry concept consists of a composition of one or more primitive geometric shapes, such as circles and line segments, with some constraints. These constraints include but are not limited to lengths, angles, and spatial relationships between the primitive shapes, for example, two perpendicular line segments or an equilateral triangle, etc.
The bottom part of the scene presents a test example, separated from the top part by a red horizontal line.
First, identify the pattern and constraints of the reference and test concepts.
Then, determine if the test example depicts the same concept as the reference examples.

You MUST provide your final answer, and the answer should follow this format: {{"answer": "yes" or "no"}}.

Geoclidean-2Shot

Given a {n}x{n} maze, where the walls are depicted by a grid of black lines between cells and along the perimeter. The maze cells are defined within the grid. The start position is marked by a red circle, and the end position by a red star. The position of each cell can be represented by coordinates (row, column), beginning from the top-left corner as (0, 0). Here, 'row' corresponds to the vertical dimension (height) of the image, and 'column' to the horizontal dimension (width).

Solve the maze by finding a path from the start position to the end position.
You MUST provide your final answer, and the answer should follow this format: {{"solution": "a list of (row, column) coordinates"}}.

Maze-Solve

Given an image containing a SVG graphic, think step by step and answer the following question:
{question}

{options}

You MUST provide your final answer, and the answer should follow this format: {{"answer": choose from "A", "B", "C", "D"}}

VGBench QA

Figure 18: Prompts for zero-shot downstream tasks with image input

The following JSON contains an approximated perception of a 2d scene. Each object (potentially including the background) is represented by a list of geometric shapes. If the object contain multiple shapes, it is a composite object. The (x, y) coordinates are in pixels, and (0, 0) is the top-left corner of the image.

--- perception ---
{perception}

Answer the following question:
Is this an acute angle or an obtuse angle?

Note that if the perception result includes a path, the angle is defined with the midpoint as the vertex, and the rays extend from the midpoint to both the head and end points. For example, if a path from A to B to C is perceived, the angle is defined as the angle between the vector BA and BC.
You MUST provide your final answer, and the answer should follow this format: {{"answer": "acute" or "obtuse"}}.

Figure 19: Prompt for task Angle Classification with Primal Visual Description perception input.

The following JSON contains an approximated perception of a 2d scene. Each object (potentially including the background) is represented by a list of geometric shapes. If the object contain multiple shapes, it is a composite object. The (x, y) coordinates are in pixels, and (0, 0) is the top-left corner of the image.

--- perception ---
{perception}

Answer the following question:
Are these two lines of equal length?

Note that perception can be noisy. A 5% offset in the measurements is acceptable. You MUST provide your final answer, and the answer should follow this format: {{"answer": "yes" or "no"}}

Figure 20: Prompt for task Length Comparison with Primal Visual Description perception input.

Given a 2d scene containing objects with the following attributes:
--- Attribute Ontology ---
- color: ['red', 'green', 'blue', 'yellow', 'magenta', 'cyan', 'gray']
- shape: ['square', 'rectangle', 'triangle', 'pentagon', 'cross', 'circle', 'semicircle', 'ellipse']

The following JSON contains an approximated perception of the scene. Each object (potentially including the background) is represented by a list of geometric shapes. If the object contain multiple shapes, it is a composite object. The (x, y) coordinates are in pixels, and (0, 0) is the top-left corner of the image.

--- perception ---
{perception}

Note that the perception can be noisy. First identify the best matching shape type and the color type from the ontology for each perceived object. For composite objects, please match the entire composition to one of the most probable objects in the ontology. Make educated guesses if necessary. Then, think step by step and answer the following question:
{question}

You MUST provide your final answer, and the answer should follow this format: {{"answer": "yes" or "no"}}

Figure 21: Prompt for task Shapeworld Spatial Reasoning (2Obj) with Primal Visual Description perception input.

Given a 2d scene containing objects with the following attributes:
--- Attribute Ontology ---
- color: ['red', 'green', 'blue', 'yellow', 'magenta', 'cyan', 'gray']
- shape: ['square', 'rectangle', 'triangle', 'pentagon', 'cross', 'circle', 'semicircle', 'ellipse']

The following JSON contains an approximated perception of the scene. Each object (potentially including the background) is represented by a list of geometric shapes. If the object contain multiple shapes, it is a composite object. The (x, y) coordinates are in pixels, and (0, 0) is the top-left corner of the image. If two objects overlap, the one with the larger index is considered to be in front of the other.

--- perception ---
{perception}

Note that the perception can be noisy. First identify the best matching shape type and the color type from the ontology for each perceived object. For composite objects, please match the entire composition to one of the most probable objects in the ontology. Make educated guesses if necessary. Then, think step by step and answer the following question:
{question}

You MUST provide your final answer, and the answer should follow this format: {{"answer": "yes" or "no"}}

Figure 22: Prompt for task Shapeworld Spatial Reasoning (MultiObj) with Primal Visual Description perception input.

Given a 2d scene containing objects with the following attributes:
--- Attribute Ontology ---
- color: ['red', 'green', 'blue', 'yellow', 'magenta', 'cyan', 'gray']
- shape: ['square', 'rectangle', 'triangle', 'pentagon', 'cross', 'circle', 'semicircle', 'ellipse']

The following JSON contains an approximated perception of the scene. Each object (potentially including the background) is represented by a list of geometric shapes. If the object contain multiple shapes, it is a composite object. The (x, y) coordinates are in pixels, and (0, 0) is the top-left corner of the image. The lowermost object has the largest y-coordinate, and the rightmost object has the largest x-coordinate.

--- perception ---
{perception}

Note that the perception can be noisy. First identify the best matching shape type and the color type from the ontology for each perceived object. For composite objects, please match the entire composition to one of the most probable objects in the ontology. Make educated guesses if necessary. Then, think step by step and answer the following question:
{question}

You MUST provide your final answer, and the answer should follow this format: {{"answer": "yes" or "no"}}

Figure 23: Prompt for task Shapeworld Superlative with Primal Visual Description perception input.

Given an image containing three boxes with light grey background, horizontally laid out. The boxes are separated by two dark grey rectangles placed vertically, which are referred to as walls. An "edge" is referred to as the boundary of the image. A "base edge" is referred to as the bottom boundary. If an object's boundary is located very close to an edge or a wall (e.g., within 10 pixels), it is considered as "touching". Each box contains a set of shapes. There are two types of images: "Tower", and "Scatter". In "Tower" images, each box contains only squares stacked in towers with up to 4 squares. In "Scatter" images, each box contains scattered objects of different sizes and shapes.

The following JSON contains an approximated perception of the image. Each object (potentially including the background) is represented by a list of geometric shapes. If the object contain multiple shapes, it is a composite object. The (x, y) coordinates are in pixels, and (0, 0) is the top-left corner of the image.

--- perception ---
{perception}

Now, identify the content in each box based on the perception result, and then think step by step to answer the following question:
{question}

You MUST provide your final answer, and the answer should follow this format: {{"answer": "yes" or "no"}}

Figure 24: Prompt for task NLVR with Primal Visual Description perception input.

The following JSON contains an approximated perception of the image. Each object (potentially including the background) is represented by a list of geometric shapes. If the object contain multiple shapes, it is a composite object. The (x, y) coordinates are in pixels, and (0, 0) is the top-left corner of the image.

--- perception ---
{perception}

The top part of the scene provides {n_shot} reference examples of a Euclidean geometry concept. A Euclidean geometry concept consists of a composition of one or more primitive geometric shapes, such as circles and line segments, with some constraints. These constraints include but are not limited to lengths, angles, and spatial relationships between the primitive shapes, for example, two perpendicular line segments or an equilateral triangle, etc.
The bottom part of the scene presents a test example, separated from the top part by a red horizontal line.
First, identify the pattern and constraints of the reference and test concepts based on the perception result. Note that the perception can be noisy. Make educated guesses if necessary.
Then, determine if the test example depicts the same concept as the reference examples.

You MUST provide your final answer, and the answer should follow this format: {{"answer": "yes" or "no"}}.

Figure 25: Prompt for task Geoclidean 2-shot Learning with Primal Visual Description perception input.

The following JSON contains an approximated perception of a {n}x{n} maze. Each object (potentially including the background) is represented by a list of geometric shapes. If the object contains multiple shapes, it is a composite object. The (x, y) coordinates for the vertices and edges correspond to the width and height position in pixels, and (0, 0) is the top-left corner of the image.

--- perception ---
{perception}

In the {n}x{n} maze, walls are depicted by a grid of black lines between cells and along the perimeter. The maze cells are defined within the grid. The start position is marked by a red circle, and the end position by a red star. The position of each cell can be represented by coordinates (row, column), beginning from the top-left corner as (0, 0). Here, 'row' corresponds to the vertical dimension (height) of the image, and 'column' to the horizontal dimension (width).

Perform the following steps to solve the maze:
(1) Infer the connectivity of the cells using a connection list. For example, a {n}x{n} maze should have a `connection_list` containing two sublisits with dimension {m}x{n} and {n}x{m}. For i in range(0, {m}) and j in range(0, {n}), `connection_list[0][i][j]` is `True` if cell `(i, j)` is vertically connected to cell `(i+1, j)` without being seperated by a wall. Similarly, for j in range(0, {m}) and i in range(0, {n}), `connection_list[1][i][j]` is `True` if cell `(i, j)` is horizontally connected to cell `(i, j+1)` without being seperated by a wall.
(2) Infer the start position and end position of the maze in the row-column format.
(3) Solve the maze by finding a path from the start position to the end position.
You MUST provide your final answer, and the answer should follow this format: {{"solution": "a list of (row, column) coordinates"}}.

Figure 26: Prompt for task Maze Solving with Primal Visual Description perception input.

Given an image containing a SVG graphic, think step by step and answer the following question:
{question}

{options}

The following JSON contains an approximated reference perception of the image. Each object (potentially including the background) is represented by a list of geometric shapes. If the object contain multiple shapes, it is a composite object. The (x, y) coordinates are in pixels, and (0, 0) is the top-left corner of the image.

--- reference perception ---
{perception}

Note that the reference perception can be noisy. Refer to the reference perception when necessary for answering the question.

You MUST provide your final answer, and the answer should follow this format: {{"answer": choose from "A", "B", "C", "D"}}

Figure 27: Prompt for VGBench-QA tasks with Primal Visual Description perception input.